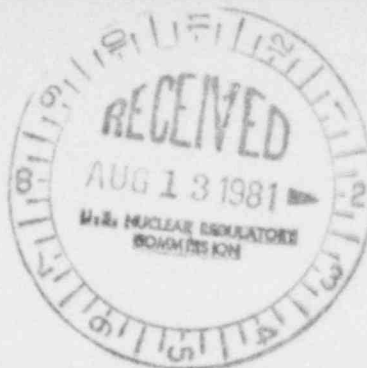


BNL-NUREG -29348

INFORMAL REPORT

LIMITED DISTRIBUTION



## AN EVALUATION OF NATURAL CIRCULATION TESTS IN FFTF

K. R. PERKINS, R. A. BARI, AND L. C. CHEN

DATE PUBLISHED - MARCH 1981

DEPARTMENT OF NUCLEAR ENERGY BROOKHAVEN NATIONAL LABORATORY  
UPTON, NEW YORK 11973



Prepared for the U.S. Nuclear Regulatory Commission  
Office of Nuclear Reactor Regulation  
Contract No. DE-AC02-76CH00016

#### NOTICE

This report was prepared as an account of work sponsored by the United States Government. Neither the United States nor the United States Nuclear Regulatory Commission, nor any of their employees, nor any of their contractors, subcontractors, or their employees, makes any warranty, express or implied, or assumes any legal liability or responsibility for the accuracy, completeness or usefulness of any information, apparatus, product or process disclosed, or represents that its use would not infringe privately owned rights.

BNL-NUREG- 29348  
INFORMAL REPORT  
LIMITED DISTRIBUTION

AN EVALUATION OF NATURAL CIRCULATION TESTS IN FFTF

K. R. Perkins, R. A. Bari, and L. C. Chen

Department of Nuclear Energy  
BROOKHAVEN NATIONAL LABORATORY  
Upton, New York 11973

March 1981

Prepared for  
U.S. Nuclear Regulatory Commission  
Washington, D. C. 20555  
Under Interagency Agreement DE-AC02-76CH00016

### ABSTRACT

Preliminary results of the FFTF natural circulation test program have been analyzed and predictions for the remaining tests have been made using DEMO-F, IANUS, and FLODISC. The post-test analysis of the secondary tests with IANUS indicate that with some adjustments the code is capable of representing the data. However, the comparisons indicate the need for some modeling refinements (more detail in the DHX, changes in the pump coastdown model, and more detail in the cold-leg modeling) in order to provide accurate predictions of secondary system transients. The secondary loop natural circulation performance (flow versus temperature gradient) compares favorably with nominal modeling, but the margin between the nominal and worst case models is found to challenge the accuracy of the experiment. The present nominal predictions for natural circulation performance in the primary loop are in good agreement with the HEDL predictions, but flow redistribution predictions appear to have important differences which are attributable to the different core representations.

## TABLE OF CONTENTS

	<u>Page</u>
ABSTRACT . . . . .	iii
LIST OF FIGURES . . . . .	v
LIST OF TABLES . . . . .	viii
1.0 INTRODUCTION . . . . .	1
2.0 PREVIOUS WORK . . . . .	2
3.0 TEST DESCRIPTION . . . . .	3
3.1 SECONDARY TESTS . . . . .	6
3.1.1 Steady-State Tests . . . . .	6
3.1.2 Transient Tests . . . . .	6
3.1.3 Comparison to Analyses . . . . .	9
3.2 PLANNED PRIMARY TESTS . . . . .	21
3.2.1 Nuclear Steady-State Tests . . . . .	21
3.2.2 Nuclear Transient Tests . . . . .	27
3.2.3 Uncertainty Analyses . . . . .	47
4.0 SUMMARY AND CONCLUSIONS . . . . .	50
REFERENCES . . . . .	52

## LIST OF FIGURES

<u>Figure</u>	<u>Title</u>	<u>Page</u>
1	Steady-state natural circulation flow in the secondary loop, calculated by IANUS and DEMO-F, Compared to HEDL Data(18) and Pretest Predictions(3).	7
2	Comparison of HEDL Heat Loss(19) Data(18) to Previous LMEC Data and the Acceptance Limit Suggested(3) by HEDL.	8
3	The nominal IANUS calculation of the DHX outlet temperature compared to the data(6) and HEDL pretest predictions(3) for the LOP from refueling conditions.	10
4	The nominal IANUS calculation of sodium flow through the DHX compared to the data(6) for the LOP from refueling conditions.	14
5	The nominal IANUS calculation of the secondary cold leg temperature at the TC location compared to the data(6) for the LOP from refueling conditions.	15
6	Schematic of the FFTF DHX operation during an LOP from refueling conditions compared to 7 node modeling in IANUS.	17
7	HEDL data for the LOP from refueling conditions compared to IANUS calculations of the secondary cold leg temperature at the TC location using the adjusted (6-pass) model of the DHX.	19
8	HEDL data for the LOP from refueling conditions compared to IANUS calculations of the secondary flow rate using the adjusted (6-pass) model of the DHX.	20
9	IANUS calculation of the secondary flow rate during pump coast-down, compared to the data and the HEDL calculations.	22
10	IANUS and DEMO-F predictions for the primary flow versus loop $\Delta T$ compared to the HEDL prediction.	24
11	FLODISC prediction of FOTA $\Delta T$ 's during steady-state testing compared to a calculation assuming no flow redistribution.	26

## LIST OF FIGURES (Cont.)

<u>Figure</u>	<u>Title</u>	<u>Page</u>
12	FLODISC nominal and worst case prediction of row 2 FOTA $\Delta T$ versus loop $\Delta T$ for steady-state testing compared to hypothetical (unmodeled) transition behavior.	28
13	Nominal IANUS prediction of core temperatures for the 5% LOP test in FFTF assuming 25 hours of prior operation at 5% power.	31
14	Nominal IANUS prediction of core temperatures for the 35% LOP test in FFTF assuming 25 hours of prior operation at 35% power.	32
15	Nominal IANUS prediction of core temperature for the 75% LOP test in FFTF assuming 25 hours of prior operation at 75% power.	33
16	Nominal and worst case IANUS prediction of core exit temperatures for the 100% LOP test in FFTF assuming 25 hours of prior operation at 100% power.	34
17	Nominal DEMO-F prediction of the core exit temperature for the average channel for the 5% LOP test in FFTF assuming 25 hours of prior operation at 5% power.	35
18	Nominal DEMO-F prediction of the core exit temperature for the average channel for the 35% LOP test in FFTF assuming 25 hours of prior operation at 35% power.	36
19	Nominal DEMO-F prediction of the core exit temperature for the average channel for the 75% LOP test in FFTF assuming 25 hours of prior operation at 75% power.	37
20	Nominal and worst case DEMO-F prediction of the core exit temperature for the average channel for the 100% LOP test in FFTF assuming 25 hours of prior operation at 100% power.	38
21	Nominal IANUS prediction of the core exit temperature for the 100% LOP test compared to the identical prediction using limiting gap conductance.	41

LIST OF FIGURES (Cont.)

<u>Figure</u>	<u>Title</u>	<u>Page</u>
22	Primary and secondary flow rates for the 35% unbalanced LOP test in FFTF assuming 25 hours of prior operation at 35% power.	45
23	Primary and secondary IHX outlet temperatures for the P-loop (representing 3 loops with pony motors off) during the 35% unbalanced LOP test in FFTF assuming 25 hours of prior operation at 35% power.	48
24	Primary and secondary IHX outlet temperatures for the I-loop (representing the 1 loop with a secondary pony motor running) during the 35% unbalanced LOP test in FFTF assuming 25 hours of prior operation at 35% power.	49

## LIST OF TABLES

<u>Table</u>	<u>Title</u>	<u>Page</u>
1	Summary of Differences for the FFTF System Models, used in the BNL Analyses, Compared to the Default Modeling in IANUS.	4
2	Summary of Flow Redistribution Modeling used in the BNL Analyses Compared to the 12-Channel FLODISC Model.	5
3	Modifications of IANUS to Simulate the Loss of Power from Refueling Conditions Experiment in FFTF.	12
4	Assumed Conditions for the Simulations of the FFTF Primary Loop, Loss-of-Power Transient Tests.	30
5	Comparison of Nominal and Worst Case Predictions of Maximum Temperatures for the FFTF 100% LOP Test after 25 hours of Full Power Operation.	40
6	Comparison Between HEDL and BNL Nominal Predictions for the 5 Percent Loss-of-Power Test in FFTF after One Hour of Prior Operation at 5 Percent Power.	44
7	Summary of BNL Test Predictions of the Maximum Temperatures for the 35% Unbalanced Loop Loss-of-Power Test in FFTF.	46

## 1.0 INTRODUCTION

As part of the Nuclear Regulatory Commission's (NRC) safety review of the Fast Flux Test Facility (FFTF) the Safety Evaluation Group at Brookhaven National Laboratory (BNL) has used pertinent computer codes to aid in evaluating some of the safety analyses presented in the FFTF Final Safety Analysis Report<sup>(1)</sup> (FSAR). The NRC's Safety Evaluation Report<sup>(2)</sup> has "...conditionally accepted the premise that there is reasonable assurance that natural circulation will be demonstrated as a viable method of removing decay heat". As part of the Natural Circulation Test Program<sup>(3)</sup> the NRC has requested<sup>(2)</sup> "...substantive verification of the mathematical models of the IANUS<sup>(4)</sup> and FLODISC<sup>(5)</sup> codes".

The purpose of the present investigation is to review the available data from the secondary system tests<sup>(6)</sup> and to provide independent predictions for the nuclear test series. The present approach has been to retain consistent modeling between the test predictions and previous safety analyses<sup>(1,7-9)</sup> and to specifically identify those modifications which are used to generate the nominal (expected) behavior.

Although the primary system tests will be the most relevant to the safety analysis, the emphasis of the present investigation has been to understand the unanticipated behavior demonstrated by the secondary system test data. The 5% transient test was performed on November 20th, 1980 but the results are not available as yet.

## 2.0 PREVIOUS WORK

There have been numerous investigations(7-11) into the natural circulation capability of fast breeder reactors. The Clinch River Breeder Reactor Project (CRBRP) used DEMO(12) to analyze the system response to LOP transients(10) and concluded that there would be adequate natural circulation to prevent boiling from occurring for the postulated LOP event.(10) However, a subsequent BNL investigation(11) indicated that the results were quite sensitive to unmodeled effects, the most significant of which was flow redistribution away from the breeding blankets. The CRBR design was modified(13) to provide back-up D.C. power for one heat transport train to ensure at least some forced circulation for the LOP event

The FFTF design does not include radial blankets and the longer primary pump coastdown is predicted(7) to give substantial margin to boiling for the postulated LOP event. However, some unmodeled effects (predominantly stratification and flow redistribution) as well as some faulted conditions(8) appear(9) to have the capability to greatly diminish the margin to boiling. Analyses at Argonne National Laboratory have indicated that severe stratification can occur in the upper plenum(14) as well as in the piping(15) at natural circulation conditions. An ongoing experimental study(16) is attempting to define the significance of three-dimensional effects in the heat exchangers.

While the limited measurement capability at FFTF precludes the likelihood of precisely defining the significance of such unmodeled effects, it is important to recognize their presence and their possible contribution to unanticipated results.

### 3.0 TEST DESCRIPTION

The stated objective of the natural circulation tests<sup>(3)</sup> is "to demonstrate the natural circulation capability of the plant and to show that performance is acceptable for all Emergency Loss-of-Power Events". A second and broader objective of the test program is to "provide necessary tools and empirical data to pertinent future breeder reactor designs to rely on sodium natural circulation as a back-up means of ensuring decay heat removal<sup>(7)</sup>". Since the test program cannot cover all hypothetical conditions, achievement of both objectives will necessitate the evaluation of computer codes which can be used to extend (interpolate and/or extrapolate) the experimental results to other conditions. We note that, although this approach appears to be necessary, it might not be sufficient with the present analytical tools and for a broad range of natural circulation conditions.

As a preliminary form of this code evaluation, test predictions have been made, using nominal and worst case modeling, to indicate the range of expected behavior. For the case of the non-nuclear tests of natural circulation in the secondary loop, the available test data<sup>(6,18)</sup> tend to agree reasonably well with the nominal modeling (as expected), but the estimated uncertainty in the data covers a large part of the difference between the worst case and nominal results. This general agreement with the nominal case cannot be construed as a rejection of the "conservative" modeling in the worst case. Rather, any modifications to the modeling must be based on statistical analysis of the data uncertainty and modeling sensitivity. This is particularly true when the models are to be used to analyze conditions out of the testing range (e.g., to analyze the behavior for a hypothetical accident). A summary of the nominal and worst case models as used for the BNL analyses are provided in Tables 1 and 2, respectively. The worst case models are intended to be conservative and are essentially those models which were used by the Project staff<sup>(7,8)</sup> and the present authors<sup>(9)</sup> to analyze loss-of-power transients in FFTF. The nominal models incorporate best-estimate modeling of key parameters which have been tested at the Hanford Engineering and Development Laboratory (HEDL) and the Liquid Metal Engineering Center (LMEC).

TABLE 1

Summary of Differences for the FFTF System Models,  
Used in the BNL Analyses, Compared to the Default Modeling in IANUS

Parameter	IANUS (Worst Case)	IANUS (Nominal)	DEMO-F (Worst Case)	DEMO-F (Nominal)
Decay Power (% of Nominal)	125	100	125	100
Core $\Delta P$ (psi, kPa)	134.4 (926.5)	112 (772)	134.4 (926.5)	112 (772)
Core Flow Exponent, $n$ ( $\Delta P = kV^n$ )	$\approx 1.82^{(a)}$	$\approx 1.82^{(a)}$	1.75	1.82
Pump Stopped Rotor $\Delta P$ (% of Nominal)	115	65	115	65
Check Valve $\Delta P$ (% of Nominal)	125	100	125	100
Upper Plenum Stratification	None	None	Immediate Stratification	Stratification Delayed by 60 Seconds
Assembly Length (m)	2.43	2.43	1.54	2.43
Reactor Days at Power	$1.0^{(b)}$	$1.0^{(b)}$	$1.0^{(b)}$	$1.0^{(b)}$
Pump Trip Delay (Sec. After Scram)	1.0	1.0	0.01	0.01
Scram Reactivity (Dollars)	18	18	18	18
Operating Power	Test Spec <sup>(b)</sup>	Test Spec <sup>(b)</sup>	Test Spec <sup>(b)</sup>	Test Spec <sup>(b)</sup>
Operating Flow	Test Spec <sup>(b)</sup>	Test Spec <sup>(b)</sup>	Test Spec <sup>(b)</sup>	Test Spec <sup>(b)</sup>
Piping Flow Exponent	$\approx 1.8^{(c)}$	$\approx 1.8^{(c)}$	1.75	1.8

Notes: (a) IANUS uses a polynomial fit of data which is approximately equivalent to an exponent of 1.82 at 3% flow.

(b) Post-test analyses will incorporate the actual days of operation, pre-test power, rod and scram delay.

(c) The piping flow exponent in IANUS changes with relative roughness of the pipe,  $\epsilon/D$ .

TABLE 2

Summary of Flow Redistribution Modeling Used in  
the BNL Analyses Compared to the 12-Channel FLODISC Model(5)

<u>Parameter</u>	<u>FLODISC - Nominal</u>	<u>FLODISC - Worst Case</u>
Flow Exponent, n ( $\Delta P = kV^n$ )	1.83*	1.75*
Upper Assembly Length (m)	2.43	1.54
Core $\Delta P$ (psi)	112	134.4
Decay Heat (Fraction of ANS)	1.0	1.25
Power/Flow (Normalized)	Variable	Variable
Transient or Steady-State	Transient	Transient
Number of Channels	12	12

---

\*Note: The flow exponent is represented approximately by a single value but actually has three components,  $k_1 V^2$ ,  $k_2 V^{1.917}$  and  $k_3 V^{1.75}$ .

### 3.1 SECONDARY TESTS

The first set of tests on the secondary system have been performed.<sup>(6)</sup> The reactor core had not yet been loaded so the heat input was provided by pump work and trace heaters. The main objectives of these tests are<sup>(6)</sup>:

(1) To determine the natural circulation flow rate in the secondary loop as a function of the temperature difference between the hot and cold leg.

(2) To verify the ability to isolate DHX modules without causing severe thermal transients.

(3) Demonstrate a secondary loop natural circulation flow start-up at refueling conditions.

(4) Measure DHX heat losses with the air path closed.

These objectives appear to have been met with only one major surprise (a much better margin to freezing than predicted for the loss-of-power from refueling conditions).

#### 3.1.1 Steady-State Tests

The two steady-state natural circulation test points are shown in Figure 1, along with the nominal and worst case calculations (post-test) using DEMO-F and IANUS. Note that the nominal calculations from both codes agree quite closely with the two data points, but when the estimated data uncertainty is considered (shown as error bars on Figure 1), there appears to be little basis for rejecting the worst case models for being too conservative. In fact, there is considerable overlap at the low-flow data point.

The steady-state dump heat exchanger (DHX) heat loss characteristics are shown in Figure 2. The HEDL<sup>(18)</sup> heat loss data are about 20% below both the previous LMEC<sup>(19)</sup> data and the acceptance limit established by the FFTF Project staff. However, the uncertainty in this data is about 20% to 40%.

#### 3.1.2 Transient Tests

Fortunately, unlike the LOP tests from operating conditions, the LOP tests from refueling conditions are very close to demonstration tests (in that pertinent parameters are identical to those hypothesized for the accident). Thus, the tests, themselves, demonstrate that freezing will not occur for the

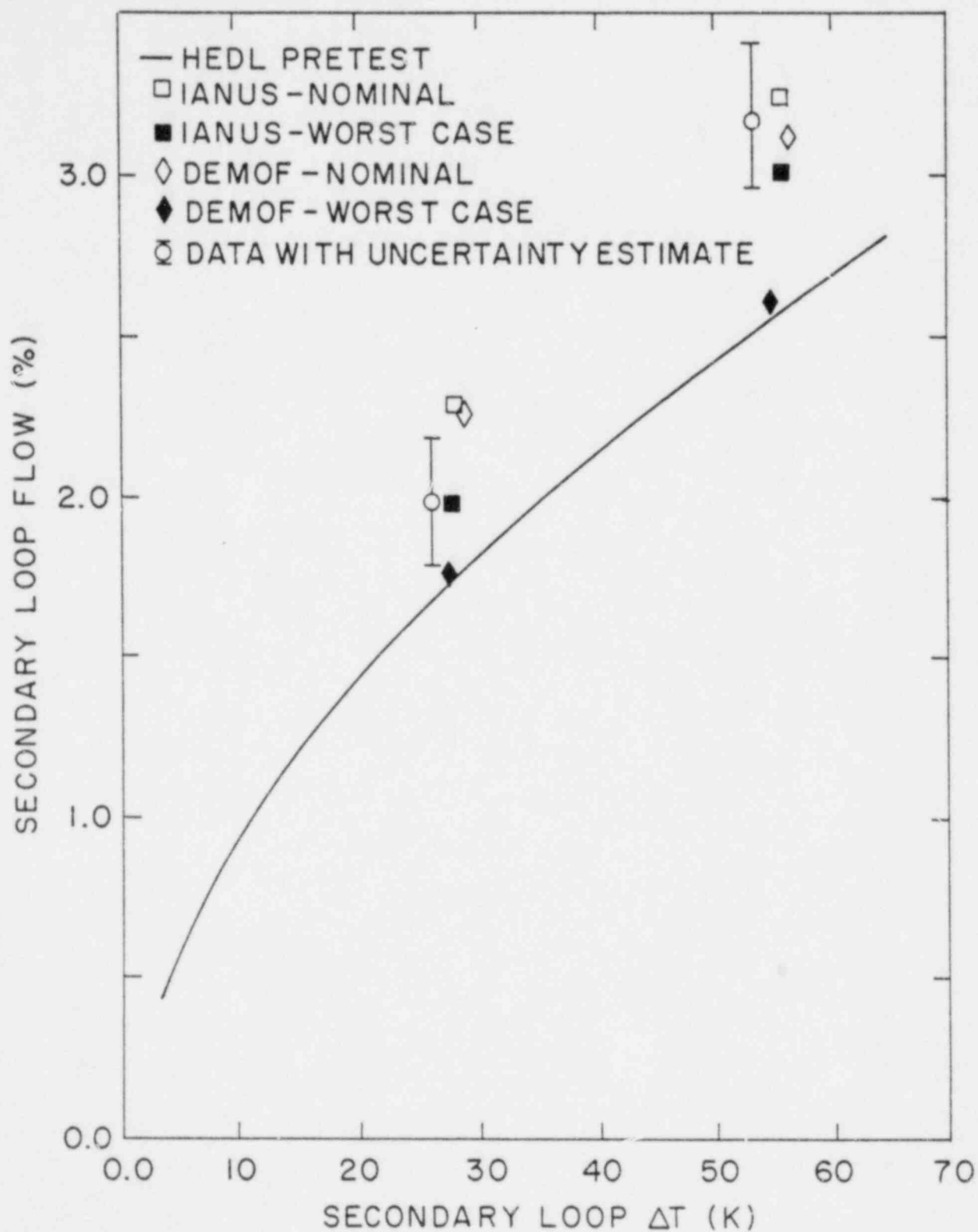


Figure 1: Steady-state natural circulation flow in the secondary loop, Calculated by IANUS and DEMO-F, Compared to HEDL Data<sup>(18)</sup> and Pretest Predictions<sup>(3)</sup>.

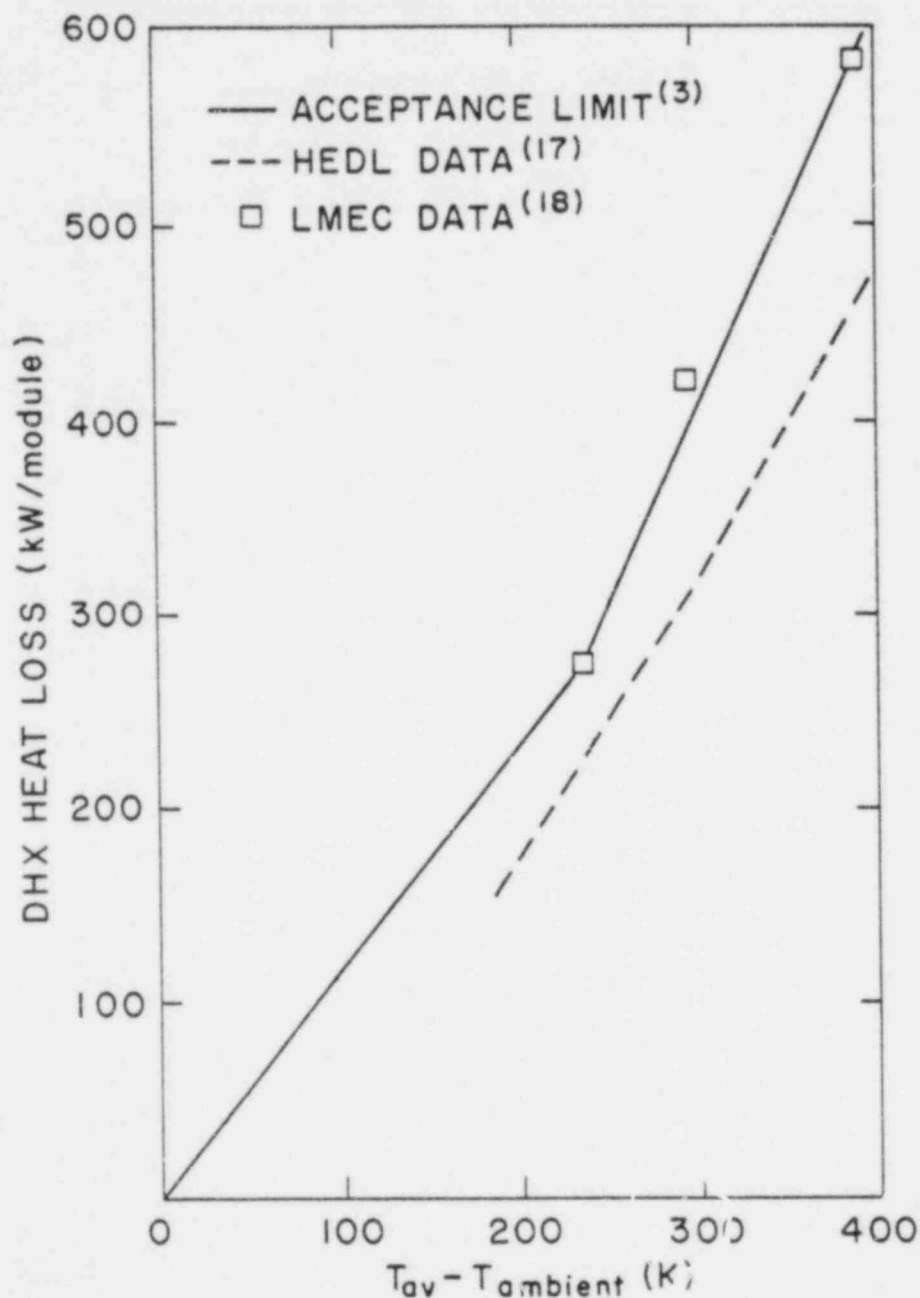


Figure 2: Comparison of HEDL Heat Loss<sup>(19)</sup> Data<sup>(18)</sup> to Previous LMEC Data and the Acceptance Limit Suggested<sup>(3)</sup> by HEDL.

given<sup>(20)</sup> hypothetical conditions (although the measurement location does not correspond precisely to the coldest point in the system).

The DHX outlet temperature measurements are shown in Figure 3, along with the nominal IANUS calculations. The minimum temperature is about 20K higher than originally predicted<sup>(3)</sup> and adds additional assurance that premature freezing will not occur for the hypothetical event.

However, it is important to note that, even with this added margin, freezing will occur eventually as the decay heat decreases and operator intervention is required to prevent all of the loops from freezing simultaneously (freezing would block all heat removal paths to the DHX).

### 3.1.3 Comparison to Analyses

While the tests of the primary system will be the most pertinent to plant safety, the data from the secondary tests will provide important verification information. The present approach has emphasized the use of the codes and models used in the previous safety analyses<sup>(1,7,8,9,19)</sup>, specifically DEMO-F, IANUS<sup>(4)</sup> and FLODISC<sup>(5)</sup>. While these codes are not intended to simulate these types of experiments, and they use relatively large amounts of computer time (due to the large time constants at natural circulation conditions), the experience gained with the verification process appears to be well worth the effort. The nominal IANUS prediction agrees surprisingly well with the two steady-state data points in Figure 1, while the worst case IANUS prediction tends to be at the lower bound of the estimated experimental uncertainty range (shown as error bars on the data points). The fact that the worst case IANUS calculation more or less bounds the data is not surprising (in fact it is rather reassuring), since the worst case model incorporates upper bound estimates of the pressure drop characteristics of the secondary system. It is more surprising to note that the original HEDL predictions<sup>(3)</sup> (also shown in Figure 1) are well below both the nominal and the worst case predictions. The large margin between the HEDL prediction and the data seems to imply that the natural circulation flow rate is much better than expected. However, most of the margin appears to be due to differences between the IANUS and the HEDL model. The data are only marginally above (the margin is approximately equal to the experimental uncertainty) the worst case prediction and very close to the nominal prediction. Similar calculations have been performed using

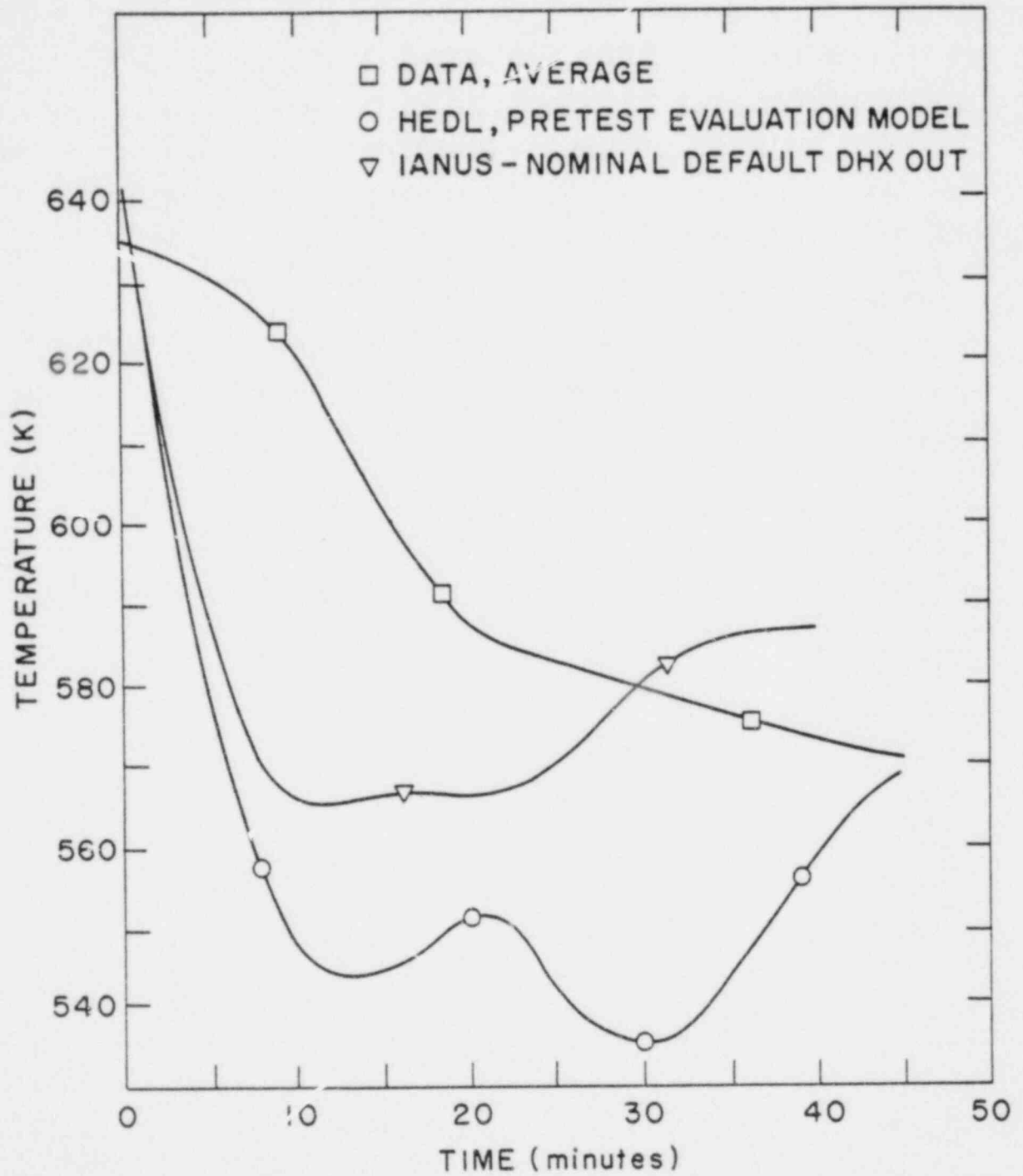


Figure 3: The nominal IANUS calculation of the DHX outlet temperature compared to the data<sup>(6)</sup> and HEDL pretest predictions<sup>(3)</sup> for the LOP from refueling conditions.

DEMO-F<sup>(9)</sup> and are also shown in Figure 1. Again, the nominal results agree quite well with the data and the worst case results tend to fall at the lower range of the estimated experimental uncertainty interval.

The behavior for the LOP from refueling conditions<sup>(6)</sup> is even more interesting in that there was a large disparity in both the shape and magnitude of the DHX outlet temperature between the nominal HEDL predictions<sup>(3)</sup> and the experiment as shown in Figure 3. Much of this disparity is said<sup>(6)</sup> to be due to neglecting the thermal capacity effects in the DHX tubes (an effect which is accounted for in IANUS). However, the post-test calculations<sup>(6)</sup> accounting for tube thermal capacity (shown in Figure 5) still demonstrated a wide disparity in shape and magnitude when compared to the data.

The present approach utilized the phenomenological modeling incorporated in IANUS to analyze the transient. DEMO-F was not used because it uses a simplified "perfect" DHX and the modifications to get DEMO-F to simulate the transient would be fairly extensive. The modifications to get IANUS to run the secondary LOP transient were minor and most of them could be accomplished by input specification. These modifications are summarized in Table 3. The first two modifications are simply manipulations of the IANUS variables to obtain the unusual boundary conditions (they are unusual only in that they are not associated with normal operating conditions and/or expected transients) associated with the secondary LOP test. The third modification can still be accomplished by a manipulation of the input, but it involves the implicit assumption that all "heat losses" are caused by leakage through the closed dampers. This leakage assumption is justified by examining the geometry of the DHX tube bundles. The tube-to-tube temperature uniformity<sup>(6)</sup> (with the exception of edge tubes) along with limited radiation view factors for interior tubes appears to be sufficient information to rule out radiation as a dominant heat transfer mechanism. There may, of course, be recirculation loops (i.e., internal natural convection), but the temperature uniformity precludes downflow within the tube bundle and the edge baffles should minimize downflow at the periphery. In any case, the assumed heat loss phenomenon (by leakage flow) results in reasonable agreement with the experiment and appears to identify the source of peculiarities in the temperature data.

TABLE 3

Modifications to IANUS to Simulate the  
Loss-of-Power from Refueling Conditions Experiment in FFTF

<u>Model</u>	<u>Change from IANUS Default Configuration</u>
Pump Work	Energy input is modeled as initial fission energy input (3.6 MW nominal) with step change to 15% of initial to hold primary system temperature constant.
Secondary Pump Trip	To get detailed hydraulics calculations all pumps are tripped with pony motor speed set to 100% of initial full flow in the primary system and 0.0% in the secondary system (this circumvents the normal trip of all pumps).
DHX Heat Loss	Fans are shut off and air flow is held constant to obtain equilibrium heat loss (1.6 MW per loop nominal at 370°C).
DHX Thermal Capacity	The modeling of the DHX in IANUS is equivalent to a 7 pass heat exchanger with most of the heat transfer taking place at the bottom pass. For realistic heat capacity and temperature distributions the air temperature at the bottom two nodes was held constant.

The IANUS nominal case DHX outlet temperature and the secondary mass flow rate are shown in Figures 3 and 4, respectively. Note that the tube bundle exit temperature (also shown in Figure 3) drops much more rapidly than the data, but this is expected since there are roughly 4 meters of pipe between the thermocouple (TC) location and the tube bundle exit. The calculated temperature at the TC location can be obtained (approximately) from the detailed printouts and this compares quite favorably in shape, but the response time is still more rapid than the data indicate, as shown in Figure 5. There are four features of the nominal IANUS calculation which merit some elaboration.

(1) The IANUS calculation yields the same shape as the data show for the first 12 minutes.

(2) The calculated temperature at 40 minutes tends to be somewhat high rather than low (as calculated by the Project staff).

(3) The IANUS calculation of the exit temperature shows a flattening off at about 15 minutes (as does the data somewhat later), but the calculation does not show the continued reduction several minutes later.

(4) Due to the imbalance in flow rates, most of the heat transfer takes place at the bottom node (of seven nodes) in the DHX. Above this node the air is too hot to provide effective cooling of the sodium.

The generally good agreement observed in (1) in shape and magnitude tends to indicate the acceptability of the convective heat loss modeling in IANUS. However, the tendency for the nominal model to overpredict the flow rate results in a relatively high outlet temperature (the product of  $\dot{m}$  and  $\Delta T$  equals the heat loss at steady-state conditions).

The overprediction of the flow rate tends to indicate that the nominal case underestimates the flow resistance at these low flow rates (as was previously observed for the steady-state data). However, it should be recognized that the calculated results are extremely sensitive to the heat loss. The value of 400 KW per module was taken from the heat loss data<sup>(18)</sup>, but these data are expected to have a large uncertainty (not yet provided by the Project).

The sudden flattening off of the DHX outlet temperature (as seen in both the data and the IANUS calculation at 15 to 20 minutes) is somewhat surprising

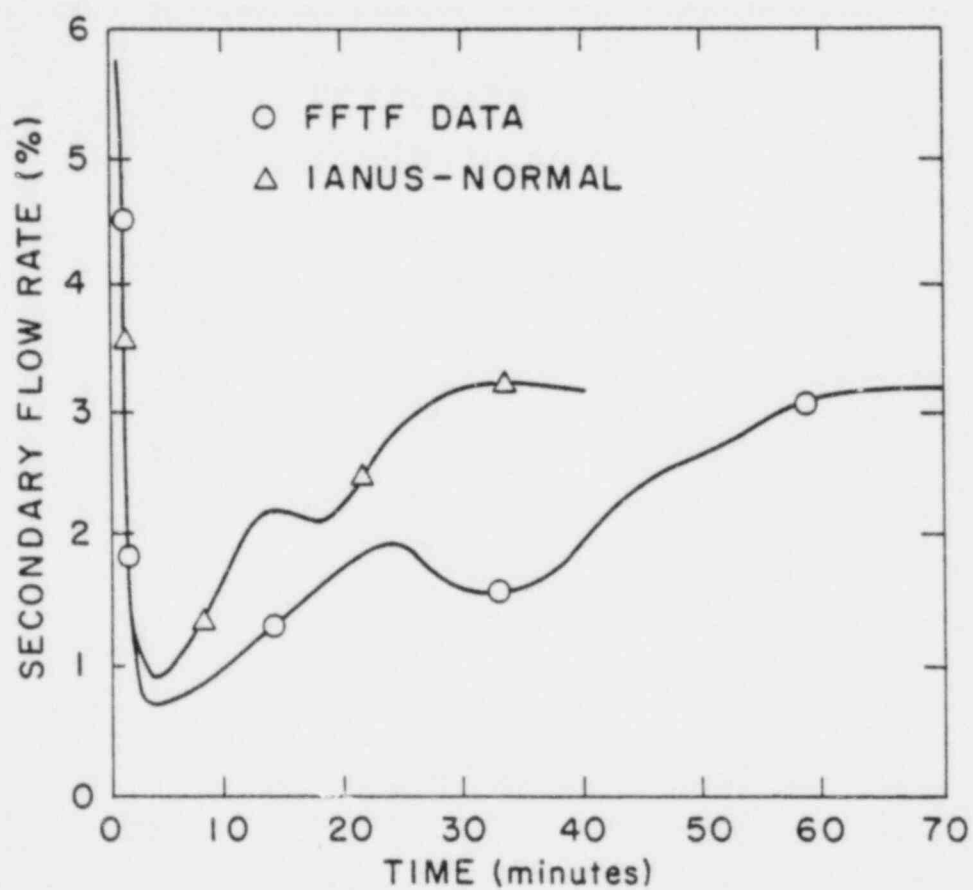


Figure 4: The nominal IANUS calculation of sodium flow through the DHX compared to the data<sup>(6)</sup> for the LOP from refueling conditions.

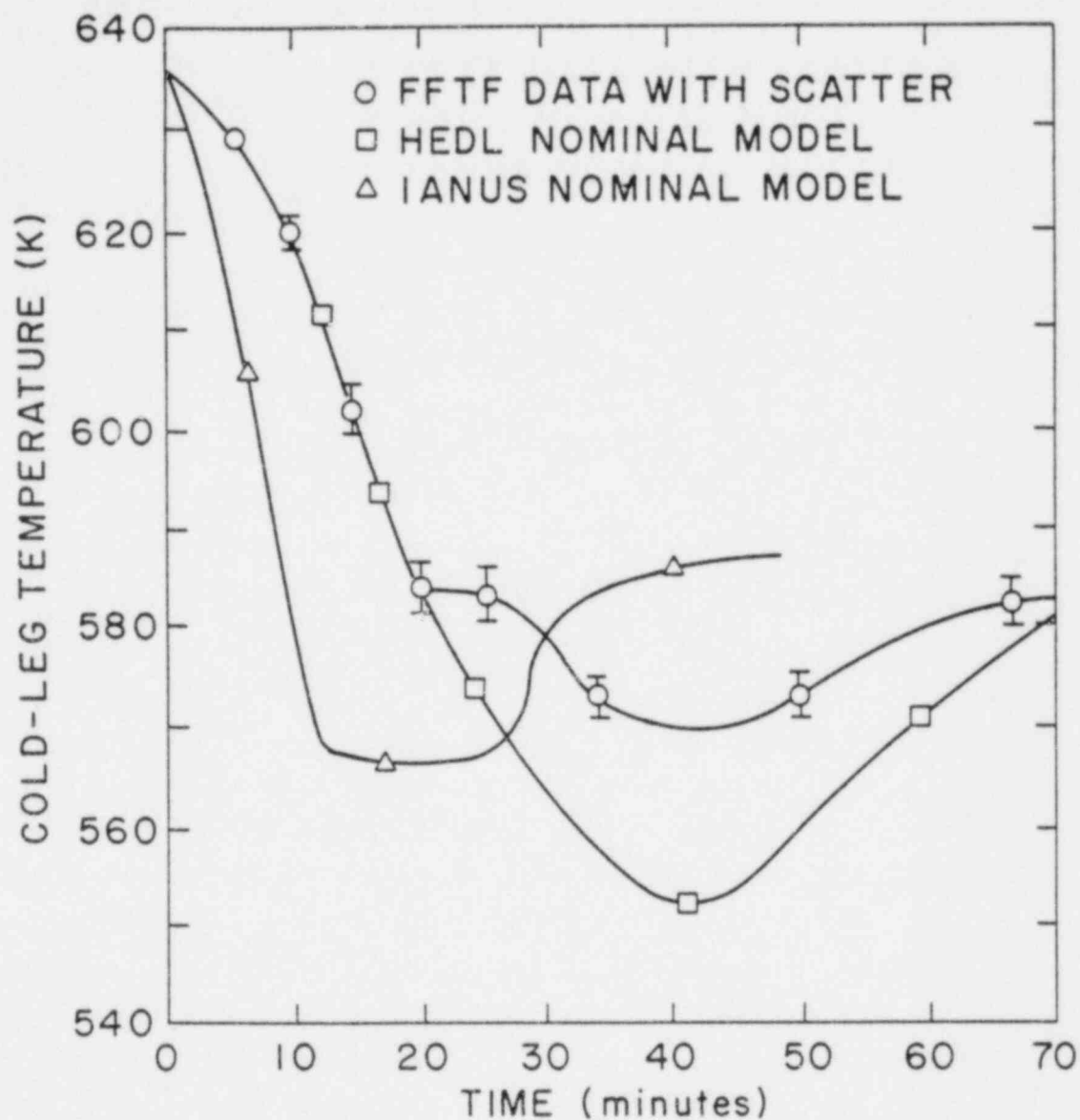


Figure 5: The nominal IANUS calculation of the secondary cold leg temperature at the TC location compared to the data (6) for the LOP from refueling conditions.

in view of the Project's calculations. However, the fourth observation (made from detailed printouts of IANUS) helps to explain the mechanism behind the dramatic change in slope of both the experiment and the calculation. With the very low air flow rate, the top six sodium nodes are essentially at the inlet temperature while most of the heat transfer takes place in the bottom node. Immediately after coastdown, the sodium flow is almost stagnant (a flow rate of about 0.5%), but the heat transfer continues to dominate in the bottom node. (Phenomenologically, the bottom node still has sufficient heat capacity to heat the air to nearly the sodium temperature.) This leads to a dramatic nonlinearity in the sodium temperature distribution. This nonlinearity is apparently not included in the HEDL model and would not be seen at the exit except that the thermal transient causes an increased buoyant head and resultant increase in mass flow (by a factor of about four). This increased flow eventually drives the hot sodium through the last node resulting in the sudden change in slope of the temperature curve. The reason for the difference in timing between the IANUS prediction and the experiment is simply that the seven node model in IANUS, in effect, models a seven-pass, counterflow heat exchanger, whereas the FFTF DHX is actually a four-pass, cross-flow heat exchanger. For the actual DHX, shown schematically in Figure 6, only the bottom pass has relatively cool inlet air flowing over it thus limiting the effective zone to 1/4 of the entire heat exchanger. Whereas, in the IANUS modeling, also illustrated in Figure 6, the bottom pass is only 1/7 of the total heat exchanger. Thus, the effective portion of the DHX model has about 1/2 (actually 4/7) of the thermal capacity and transport time of the effective portion of the FFTF DHX. While the present authors have not attempted to do so, it is fairly obvious that the agreement between the code and the experiment can be greatly improved by changing the modeling to a cross-flow representation with noding capability in multiples of 4.

In an attempt to demonstrate the importance of the nonlinear temperature distribution on the ensuing transient, the air-side temperature calculations were overridden to hold the air temperature to a constant value (175°C) for the bottom two nodes. Thus, the length of the effective heat exchanger is doubled to 11.1 m (as opposed to the actual length of the first pass of 9.7). This modeling would be expected to result in a more consistent response time between the model and the experiment.

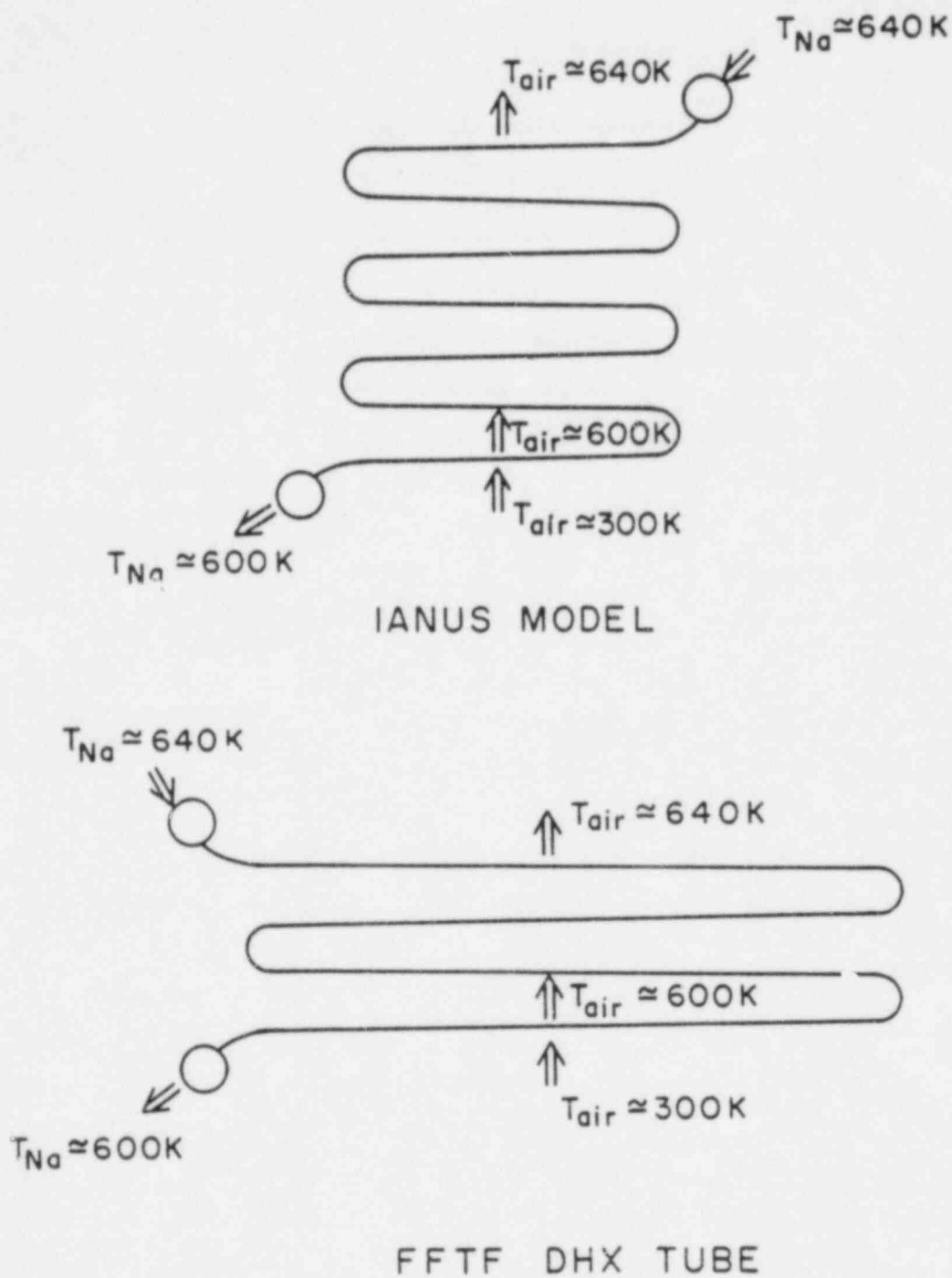


Figure 6: Schematic of the FFTF DHX operation during an LOP from refueling conditions compared to 7 node modeling in IANUS.

Several calculations were performed with this adjusted (6 pass) model. The chronology of these calculations is not particularly relevant, but it is interesting to point out the good agreement which can be achieved with this adjusted model. The preliminary calculations indicated that about 1/3 of the heat losses occur above the bottom pass of the DHX. While the precise distribution of this remaining heat loss does not appear to be important for the present calculations, it was assumed to be radiation from the top pass of the heat exchanger. With this heat loss distribution and the experimentally determined heat loss, the worst case (maximum flow resistance) model gives good agreement with the data as indicated in Figures 7 and 8. The tendency for the calculations to rise back to equilibrium more quickly (at about 60 minutes) than the data indicate is probably due to one or more factors, including: numerical diffusion of heat in the cold leg; thermal stratification; errors in geometry including lack of pump tank; or the coarse nodalization of the DHX. (Each of the seven nodes in the DHX model represents about 5.6 m of tubing while the outlet temperature is an average of about 15 m of pipe.) Note that the IHX utilizes an optional number of nodes and that 21 appears to be a minimum number to follow rapid thermal transients.

The nominal IANUS calculation (not shown) with the modified (6 pass) DHX consistently overpredicts the flow rate and underpredicts the temperature drop. However, by increasing the assumed heat loss to the acceptance limit, the calculated exit temperatures show improved agreement with the data (as shown in Figure 7). However, this good agreement in temperature is obtained at the expense of the flow rate. Thus, the nominal flow rate calculations are considerably above the data shown in Figure 8. The tendency for both the nominal and worst case IANUS models to predict high flow rates after about 25 minutes (in spite of following the DHX thermal transient to about 35 minutes) leads us to the conclusion that the thermal transport or geometry in the cold leg is incorrectly modeled. It is also noteworthy that the adjusted HEDL model does show consistent transient response with both the flow and temperature data. This tends to indicate that there are differences in the geometry and/or thermal transport for the cold leg which do not show up during steady-state (when the cold leg is at uniform temperature). Informal discussions with HEDL personnel indicate that the only known difference in the modeling of the cold leg is the inclusion of the pump tank in the HEDL model.

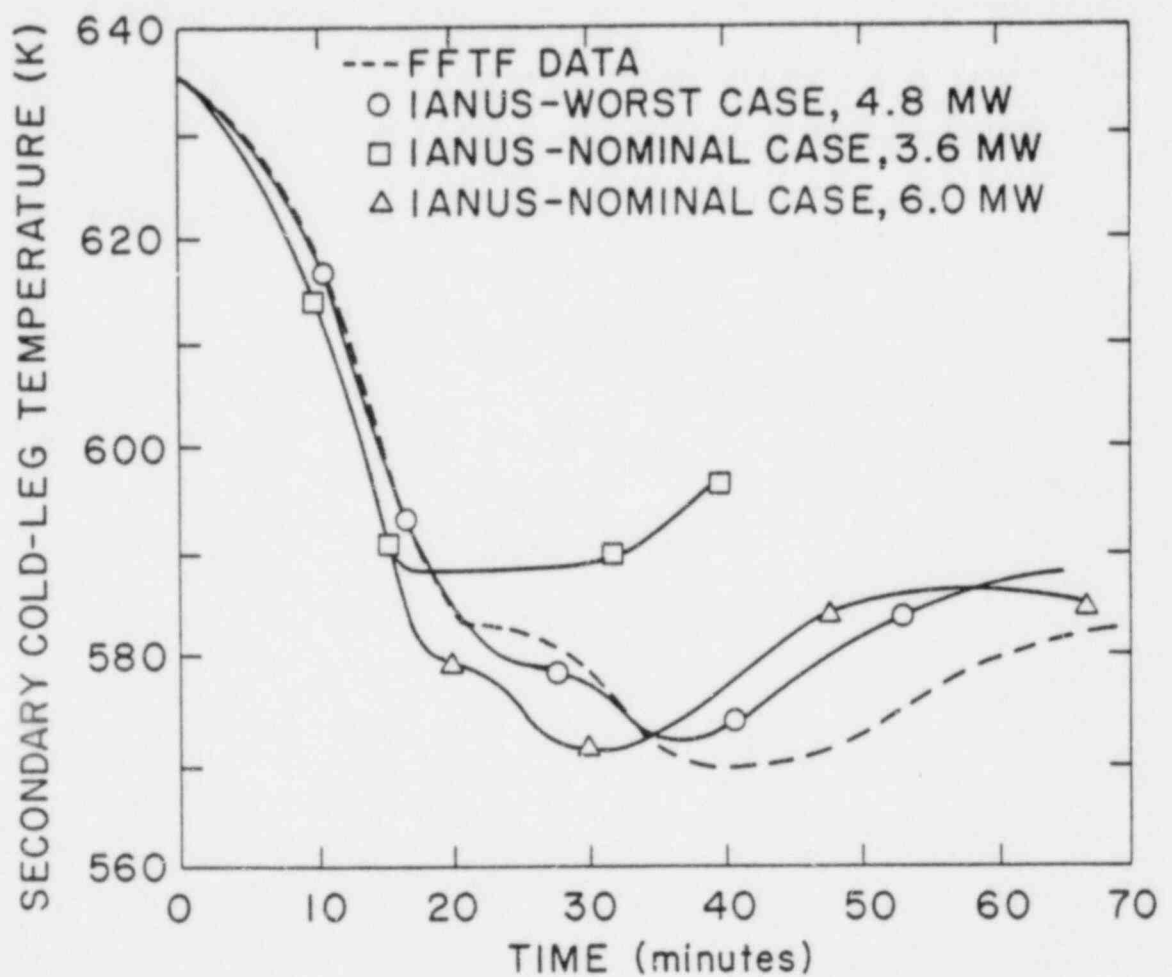


Figure 7: HEDL data for the LOP from refueling conditions compared to IANUS calculations of the secondary cold leg temperature at the TC location using the adjusted (6-pass) model of the DHX.

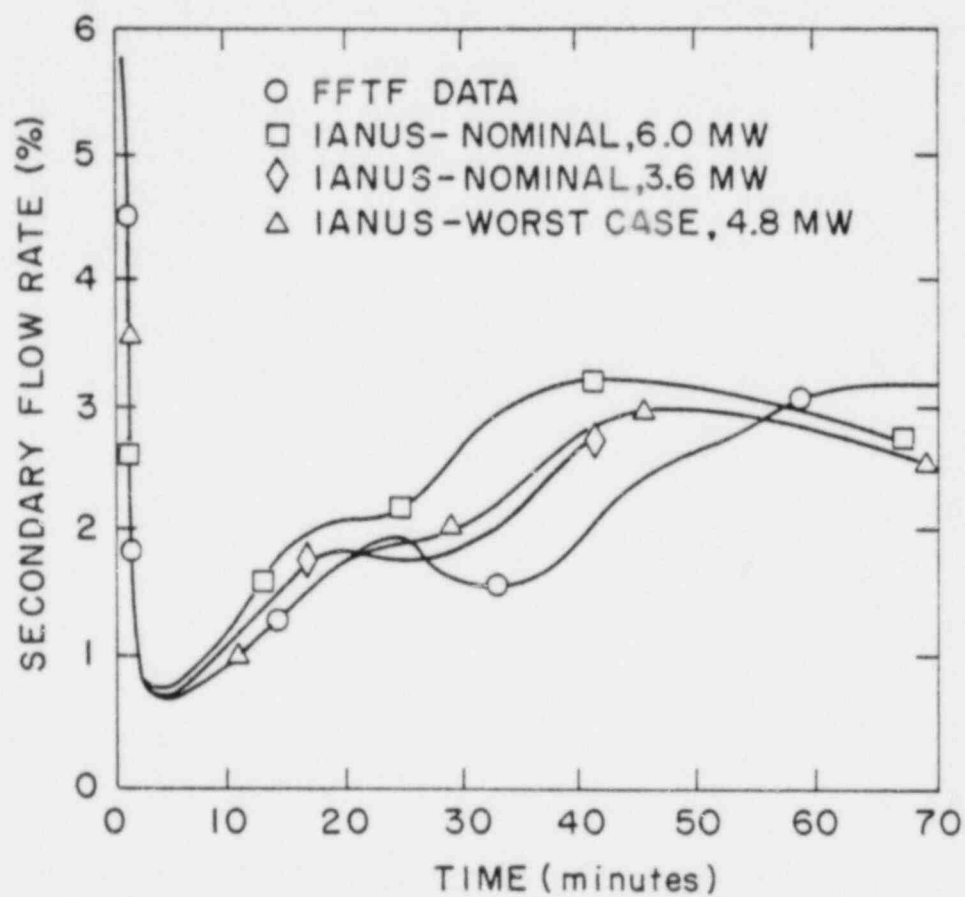


Figure 8: HEDL data for the LOP from refueling conditions compared to IANUS calculations of the secondary flow rate using the adjusted (6-pass) model of the DHX.

During the initial coastdown, (shown in Figure 9) both the worst case and nominal case IANUS underpredict the loop flow rate. The DEMO-F calculations (not shown) were fairly consistent with a tendency to be slightly lower than IANUS. It should be recognized that both the "nominal" and "worst case" models are somewhat conservative predictors of the mass flow rate during pump coast-down (as they are intended to be). This slight conservatism in flow rate can be eliminated by adding an inertial term to account for the sodium in the pump impeller (as was apparently done for the HEDL calculations).

### 3.2 PLANNED PRIMARY TESTS

As previously mentioned, the emphasis of the present report is on the evaluation of the available secondary test data. However, several illustrative predictions of the primary tests are included to emphasize a key point, specifically:

There is a very limited margin between the worst case calculations and the nominal calculations. It is felt that the verification program should acknowledge uncertainties in the data and attempt to attach some confidence level to the conservative model, or equivalently, attempt to realistically quantify the uncertainty band (not simply data scatter) around modified models.

It should be recognized that many details of the natural circulation tests from nuclear power may change significantly from the planned conditions (delay before pump trip, decay power, control reactivity, environmental temperature, etc.). In fact, the limited DHX capability indicates that the 100% power test cannot be run unless the inlet air temperature is considerably below the design temperature of 32°C.

In any case, no attempt has been made to "fine tune" the analyses to imprecisely defined test conditions. The present predictions are presented to illustrate existing differences between the Project's models and the present models as well as to indicate the magnitude of the limited margin between the predictions using the nominal modeling, and predictions using the worst case modeling.

#### 3.2.1 Nuclear Steady-State Tests

The steady-state primary tests are scheduled to be completed early in 1981. As with the secondary tests, the primary steady-state tests will provide

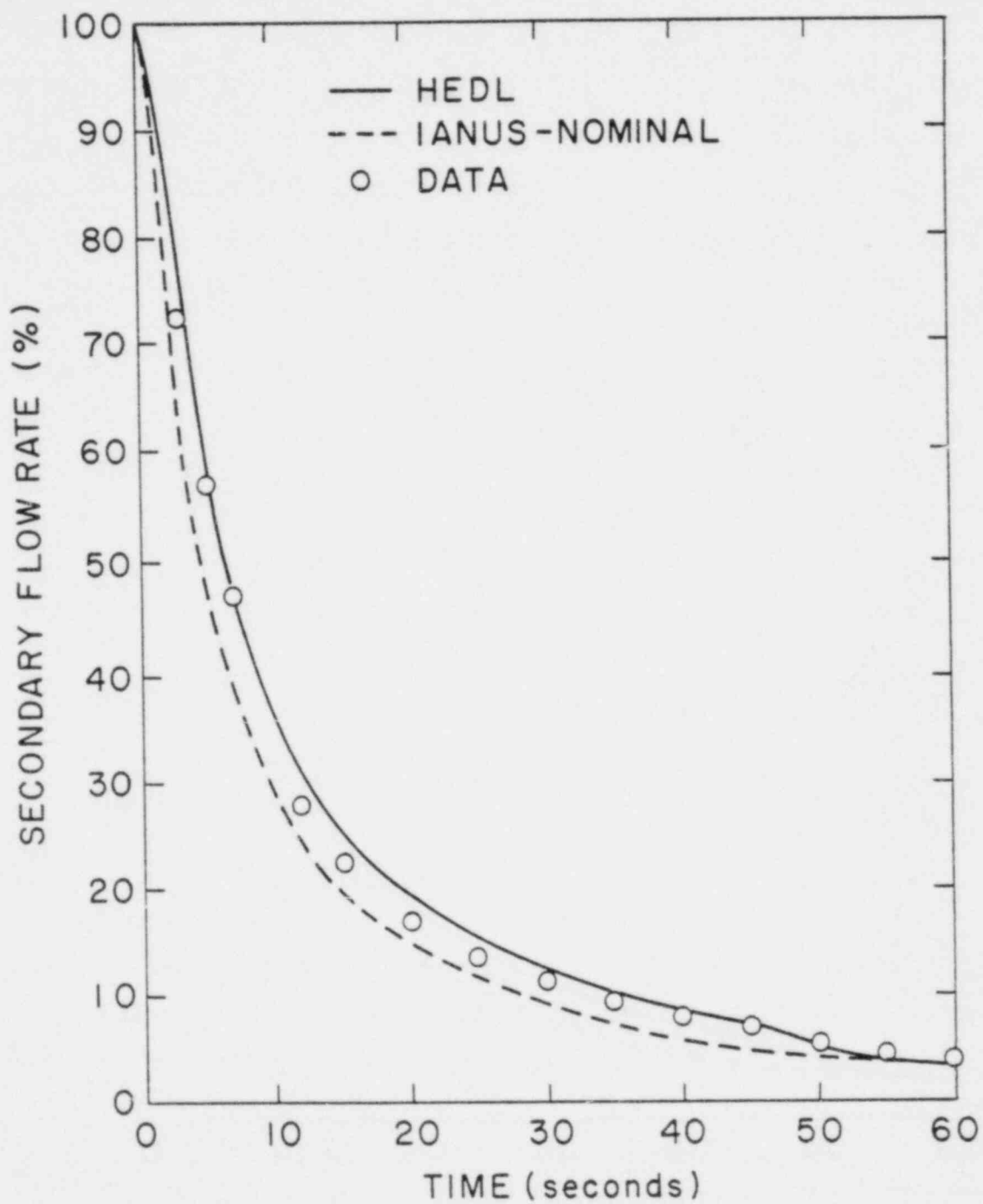


Figure 9: IANUS calculation of the secondary flow rate during pump coastdown, compared to the data and the HEDL calculations.

important verification of the integral pressure loss characteristics of the primary loop. Since the core  $\Delta P$  tends to dominate the pressure losses even at low flow rates, these measurements will provide important (albeit indirect) confirmation of the estimated pressure loss characteristics at low flow rates.

The nominal and worst case DEMO-F and IANUS predictions of the mass flow versus loop  $\Delta T$  in the primary system along with the HEDL prediction are shown in Figure 10. Somewhat surprisingly (in light of the disagreement on the secondary side), the nominal DEMO-F and IANUS predictions are in substantial agreement with the HEDL calculations. This agreement does not necessarily mean that all the flow resistance models are identical for each of the predictions, it simply reflects the predominance of the precisely defined core pressure drop (i.e., the nominal core pressure drop of 770 kPa is defined by extensive experimentation and has been used identically in each calculation) in the overall pressure loss estimate. The most important aspect of the comparison is that the worst case predictions are only about 10% lower than the nominal predictions. Given the inherent difficulties in making measurements in a nuclear environment (with thermal and irradiation induced drift) it is expected that it will be extremely difficult to discriminate between the nominal and worst case models. For example, a flow measurement which is accurate to within 0.2% of full scale gives rise to an uncertainty of about 10% at natural circulation conditions.

The steady-state natural circulation tests will also provide important data to verify flow redistribution predictions. As pointed out previously<sup>(21)</sup> the flow redistribution model is one of the most important aspects of the verification program since it provides the basic mechanism to extrapolate the computer code prediction of the average temperature rise to the statistically worst assembly (the "hot" assembly having a power-to-flow ratio 55% above the average assembly). The row 2 fuels-open-test assembly (FOTA) will provide an intermediate point (with a power-to-flow ratio 27% above the average) for verification, but the model must remain on sound phenomenological ground in order to perform the extrapolation with confidence. While IANUS and DEMO-F do not account for flow redistribution explicitly, the beneficial effects (the effects are beneficial in that the hot channel factor is reduced) of flow redistribution are accounted for in the flow-dependent "maldistribution"

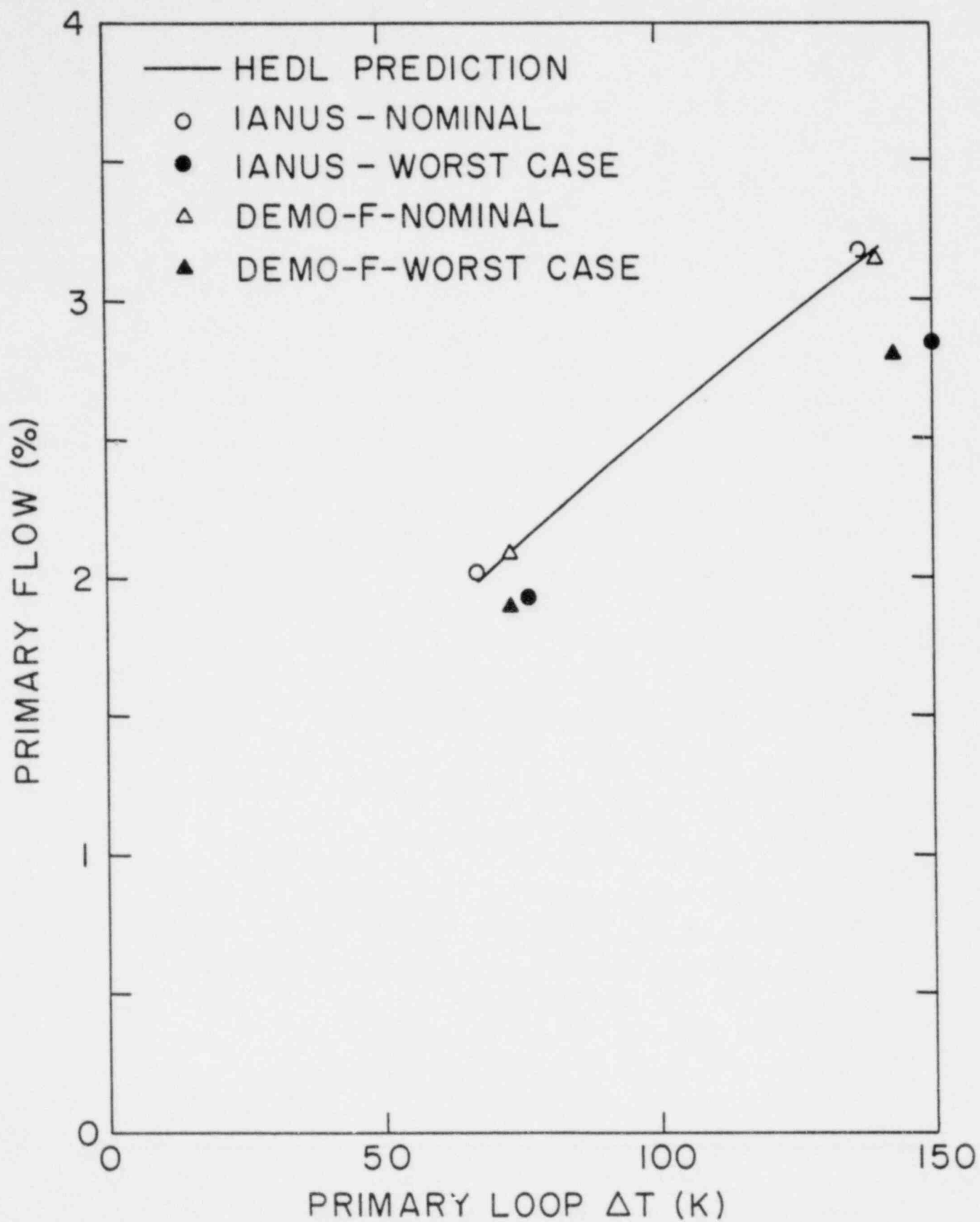


Figure 10: IANUS and DEMO-F predictions for the primary flow versus loop  $\Delta T$  compared to the HEDL prediction.

factor. Buoyancy-induced redistribution is a real phenomenon, but the effects of flow transitions in the orificing may negate the beneficial effects.

As with the secondary tests, only careful application of uncertainty analysis can be expected to reduce the margin between the nominal and worst case models. In fact, for the steady-state tests, the conservative flow redistribution model (as used in IANUS) and the nominal model are essentially equivalent in that the main conservatism built into the IANUS model is to limit the power-to-flow ratio to be at most equal to 1.0. Since the power-to-flow ratio is expected to be less than 1.0 for all the steady-state tests, the margin between the conservative model and the nominal model is zero. Obviously, the data cannot distinguish between identical models and verification of the conservatism in the IANUS flow distribution model will require transient data with a high power-to-flow ratio.

As an indication of the difficulties inherent in verifying flow redistribution models, the prediction of the nominal  $\Delta T$  across the row 6 FOTA versus the row 2 FOTA  $\Delta T$  is shown in Figure 11. While these two assemblies have significantly different power levels (6830 KW for the row 2 FOTA versus 5080 for the row 6 FOTA), the flow orificing is designed to keep the  $\Delta T$  across the two assemblies nearly equal at full power conditions. The result is that the buoyancy-induced flow redistribution is predicted to be nearly the same for both assemblies and the row 2  $\Delta T$  is predicted to be only 10% higher than the row 6  $\Delta T$  as shown. If there were no flow redistribution, the row 2  $\Delta T$  would be 9% higher than the row 6  $\Delta T$  as shown in Figure 11. Thus, the margin between the expected flow redistribution and no flow redistribution translates into a 1.0% difference in  $\Delta T$ . Obviously, when one considers the measurement uncertainties (power level,  $\Delta T$  and  $\Delta P$ ) it will be difficult to use this comparison as a verification tool.

It appears much more productive to compare FOTA  $\Delta T$  to the total loop  $\Delta T$ . Since flow distribution to the loop remains constant (at 100%), any significant (larger than measurement uncertainties) change in the  $\Delta T$  ratio can be ascribed to flow redistribution effects (although it still may be difficult to determine which effects are due to buoyancy-induced redistribution and which effects are due to friction-induced redistribution). For this case the nominal FLODISC model predicts that the row 2  $\Delta T$  will be about 20% higher than the loop  $\Delta T$  as

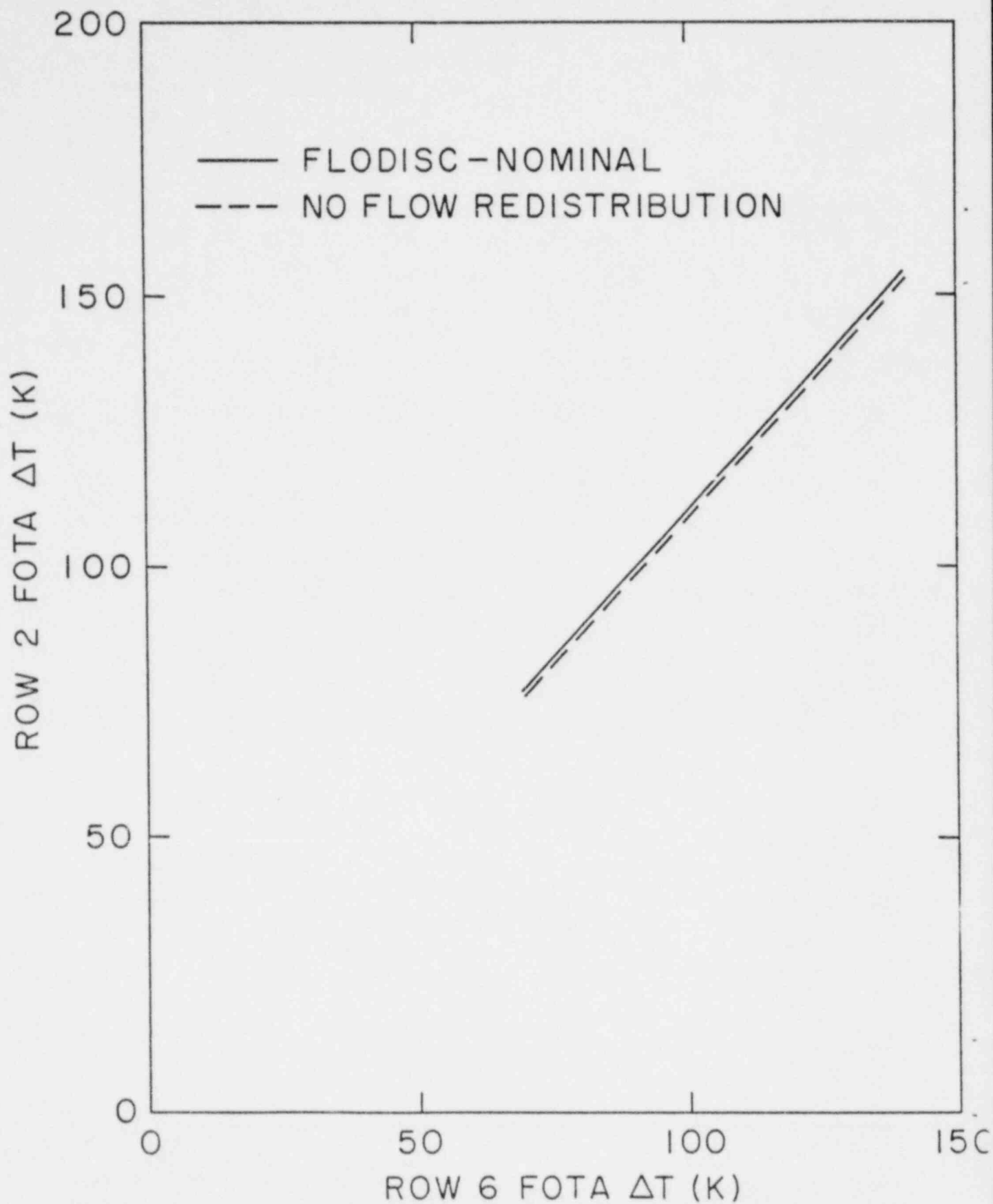


Figure 11: FLODISC prediction of FOTA  $T$ 's during steady-state testing compared to a calculation assuming no flow redistribution.

indicated in Figure 12. This is about 25% better than the case of no flow redistribution. It is interesting to note, however, that while the 25% margin is likely to be larger than the experimental uncertainty, the adverse orificing effects at low flow (the orificing is designed for full flow) have the potential to negate this margin. For example, the worst case model suggested by Perkins and Bari<sup>(20)</sup> (see Table 2) predicts that in the limiting case there could be nearly no flow redistribution. This bounding estimate does not imply that any adverse flow redistribution will show up as a uniform departure from the nominal predictions. Rather, such adverse behavior is expected to show up over a limited range (representative of turbulent-to-laminar transition region) as indicated for a hypothetical experiment by the dashed line in Figure 12. Thus, it will be important to evaluate the data over the full range of the experiment in order to verify the flow redistribution models. The tendency to reject data as spurious if it does not fit the model must be avoided. This is particularly true if one is to attempt to apply the data obtained from a few test assemblies (the most reliable flow redistribution data is expected to come from the three FOTA's) to all 76 assemblies in the reactor. While there are only three orifice zones in FFTF, the "orifices" themselves are simply holes drilled in reflector blocks and they cannot be expected to have the reproducible characteristics of a standard, sharp-edged orifice.

### 3.2.2 Nuclear Transient Tests

The transient natural circulation tests will provide important data for verifying the computer codes at conditions approaching the conditions of the postulated loss-of-power event. While the tests are programmed to gradually lead up to the full power tests with increasing levels of confidence in the predictive tools, it is clear that even the full power test is not a demonstration test for the postulated events (i.e., the worst case LOP events<sup>(7,8,20)</sup>). The greatest utility of the tests will be for verification of the codes used in safety analyses. The codes can then be used to extend results (with adequate allowance for experimental uncertainties) to the specific conditions of postulated accidents. In the particular instance of the worst case LOP event<sup>(7)</sup>, the essential variables which require extrapolation beyond the data base are the power level at transition to natural circulation (from about 2%, depending on power history, to 3.5%) and the power-to-flow ratio (from about 1.27 for the FOTA to 1.55 for the hypothetical accident).

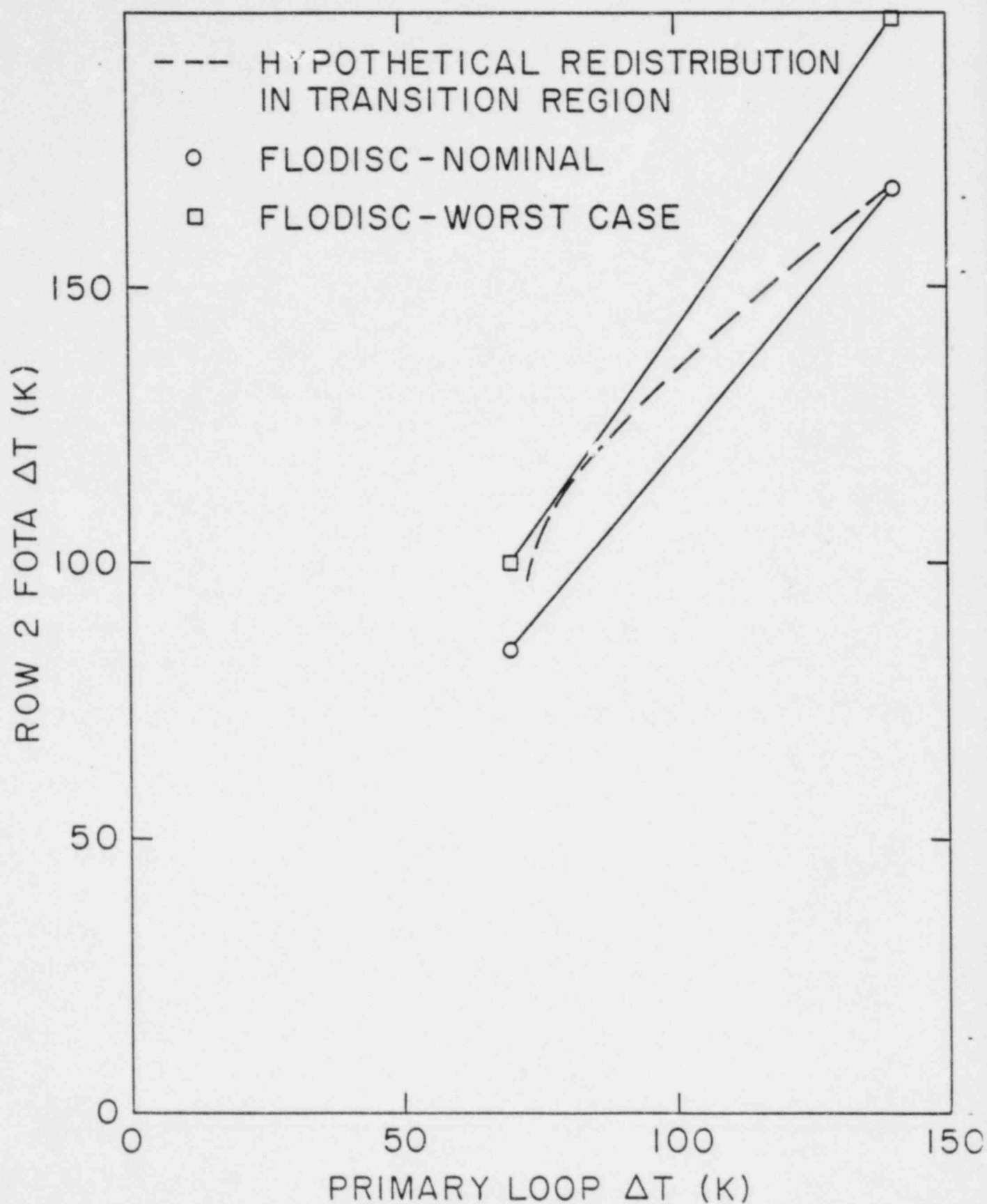


Figure 12: FLODISC nominal and worst case prediction of row 2 FOTA  $\Delta T$  versus loop  $\Delta T$  for steady-state testing compared to hypothetical (unmodeled) transition behavior.

The nominal IANUS model (see Table 1) has been used to predict the core outlet temperature for the 5%, 35%, 75% and 100% tests as shown in Figures 13 through 16. The conditions for each prediction are described in Table 4. The intent of these predictions is not to show details of the predicted behavior since the initial conditions (particularly operating history) may change enough to make the details irrelevant. Rather, the predictions are included to:

- (1) show the anticipated range of behavior (related to the requirements for experimental accuracy);
- (2) benchmark the behavior of the existing models in IANUS; and
- (3) establish whether significant differences exist between the FFTF Project's predictions and the present predictions using modeling that is theoretically identical.

The most important aspect of these predictions is the margin between the worst case and the nominal predictions. Even for the 100% power case the peak worst case core outlet temperature is only 35 K higher than the nominal prediction as shown in Figure 16. As with the other phases of the test program, this limited margin is expected to challenge the accuracy of the experimental results.

Predictions, for the identical cases using the nominal and worst case models for DEMO-F, have been made and the results are presented in Figures 17 through 20. While it is not obvious from the plots (due to the slightly different graphics routines which generated the plots), the nominal cases for the DEMO-F and IANUS predictions are essentially identical.

The worst case DEMO-F prediction at 100% power (also shown in Figure 20) is significantly worse (by about 20K) than the worst case IANUS prediction due to the presence of upper-plenum stratification and the bounding core  $\Delta P$  used in the DEMO-F worst case model. At this time neither worst case model can be recommended over the other, except to say that the DEMO-F model is more conservative. The utility of the different models is expected to be seen in the post-test evaluations in that detailed data comparisons will aid in establishing the significance of the different modeling approaches. For instance, comparisons of core outlet and vessel outlet temperatures with DEMO-F calculations can be expected to establish the importance of stratification in the upper plenum (which is not modeled in IANUS).

TABLE 4

Assumed Conditions for the Simulations  
of the FFTF Primary Loop, Loss-of-Power  
Transient Tests

Test	Initial Power (% of Design)	Hours of Operation at Initial Power	Initial Flow (% of Design)	Core Inlet Temperature (K)
5%	5	25	75	583.5
35%	35	25	75	583.5
35% (Unbalanced*)	35	25	75	583.5
75%	75	25	75	634.3
100%	100	25	100	634.3

\* Informal discussions indicate that the 35% test will actually be run in an unbalanced configuration with one secondary pony motor remaining active.

# NAT CIRC ON PRIMARY LOOP 5% POWER 75% FLOW

CASE NUMBER 4041

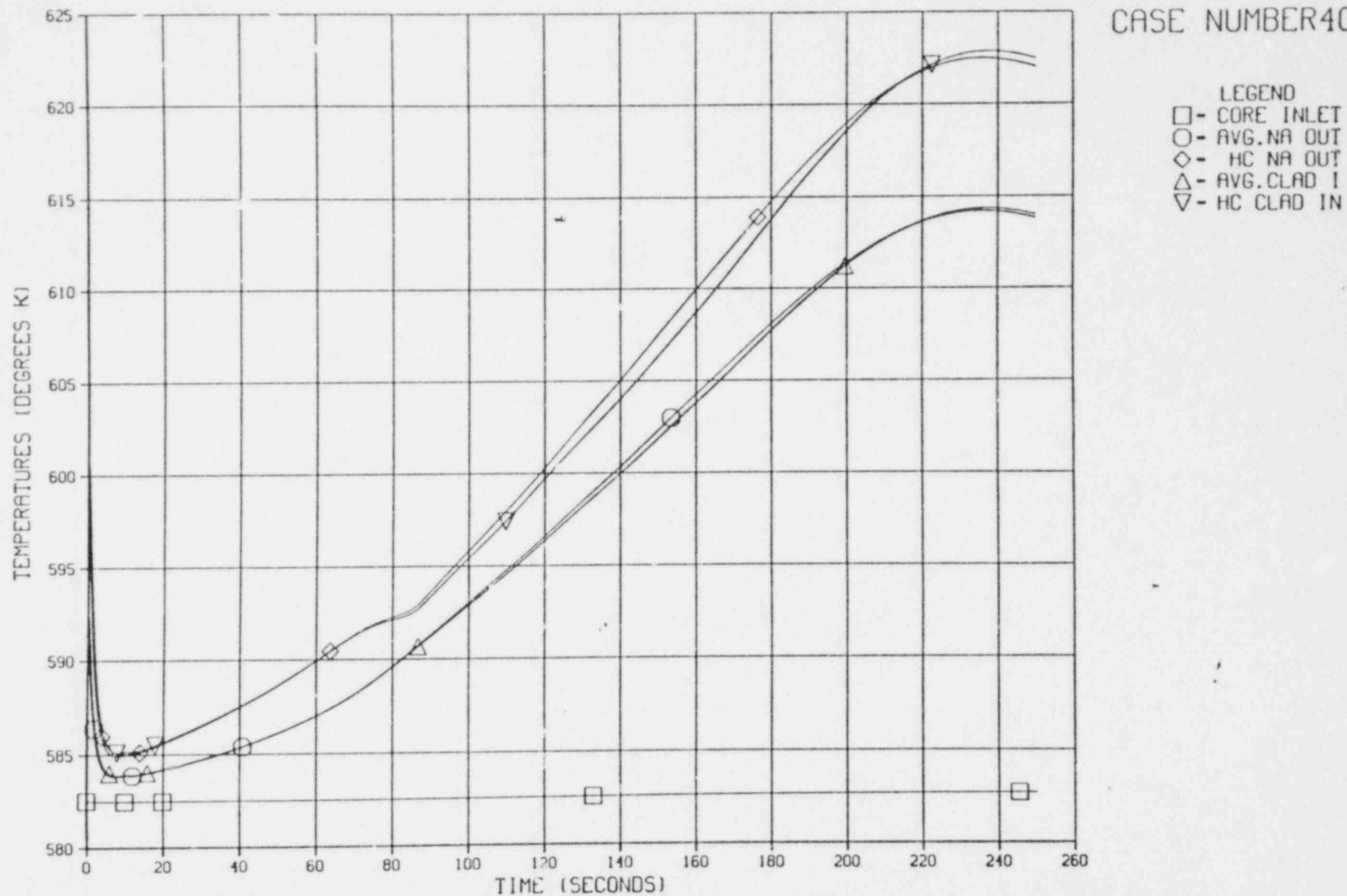


Figure 13: Nominal IANUS prediction of core temperatures for the 5% LOP test in FFTF assuming 25 hours of prior operation at 5% power.

# DETAILED CORE TEMPERATURES (3 X 5 CORE USED)

NAT CIRC ON PRIMARY LOOP 35% POWER 75% FLOW

CASE NUMBER 3040

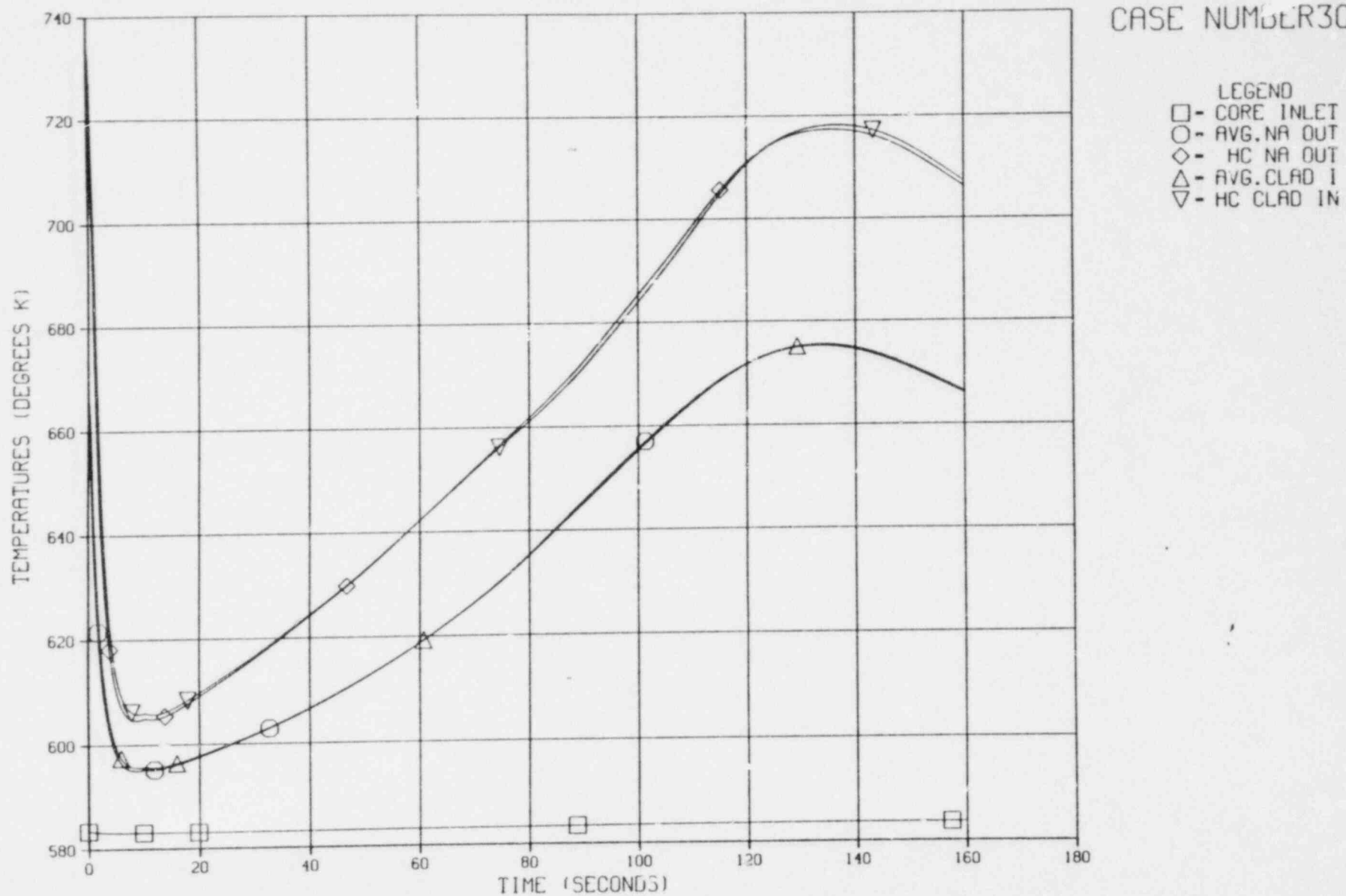


Figure 14: Nominal IANUS prediction of core temperatures for the 35% LOP test in FFTF assuming 25 hours of prior operation at 35% power.

DETAILED CORE TEMPERATURES (3 X 5 CORE USED)  
75% LOP TEST AT 25 HOURS

CASE NUMBER 3039

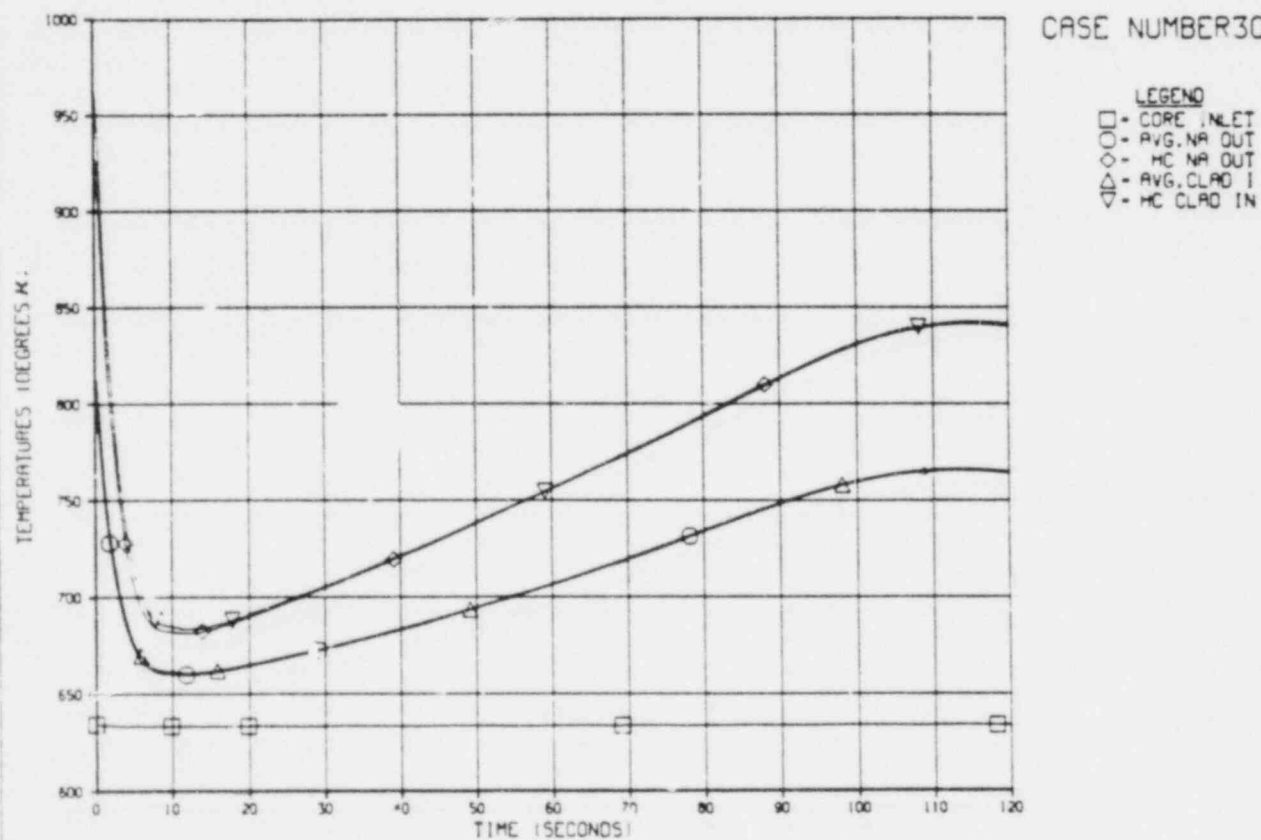


Figure 15: Nominal IANUS prediction of core temperature for the 75% LOP test in FFTF assuming 25 hours of prior operation at 75% power.

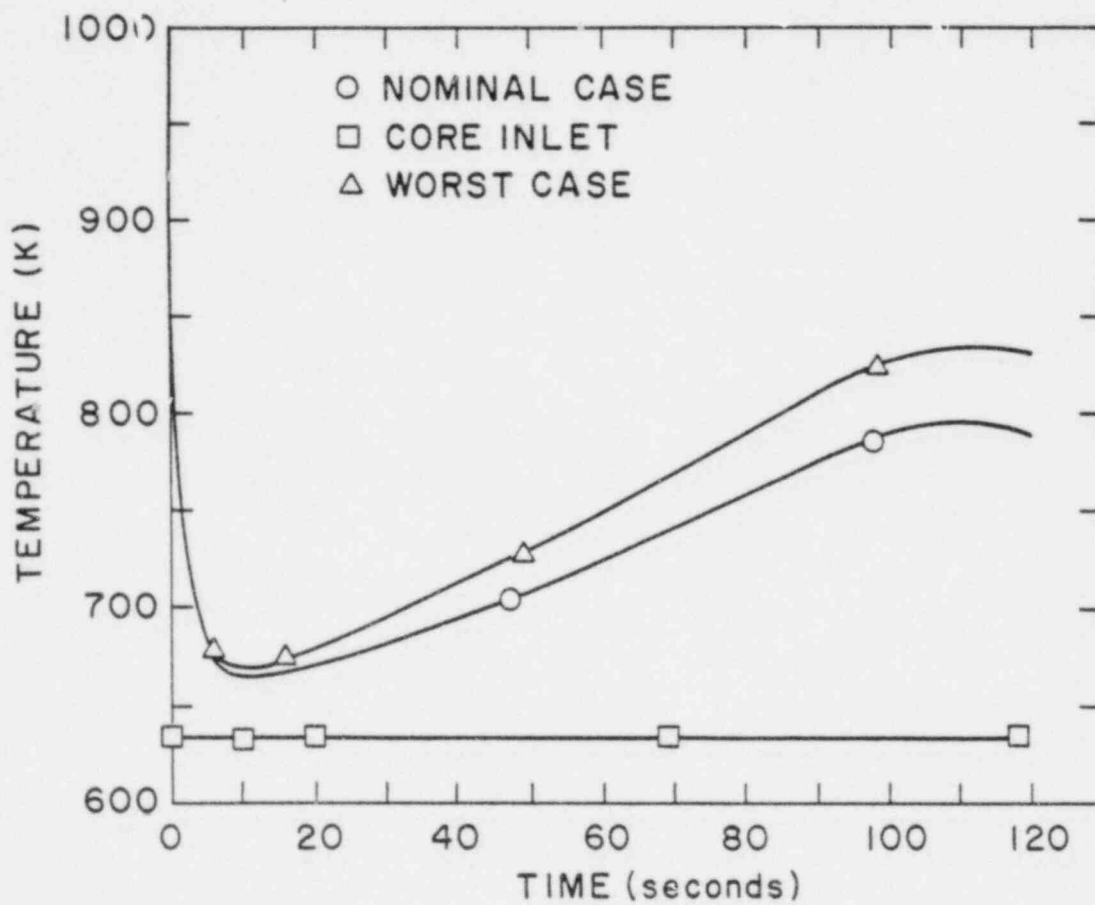


Figure 16: Nominal and worst case IANUS prediction of core exit temperatures for the 100% LOP test in FFTF assuming 25 hours of prior operation at 100% power.

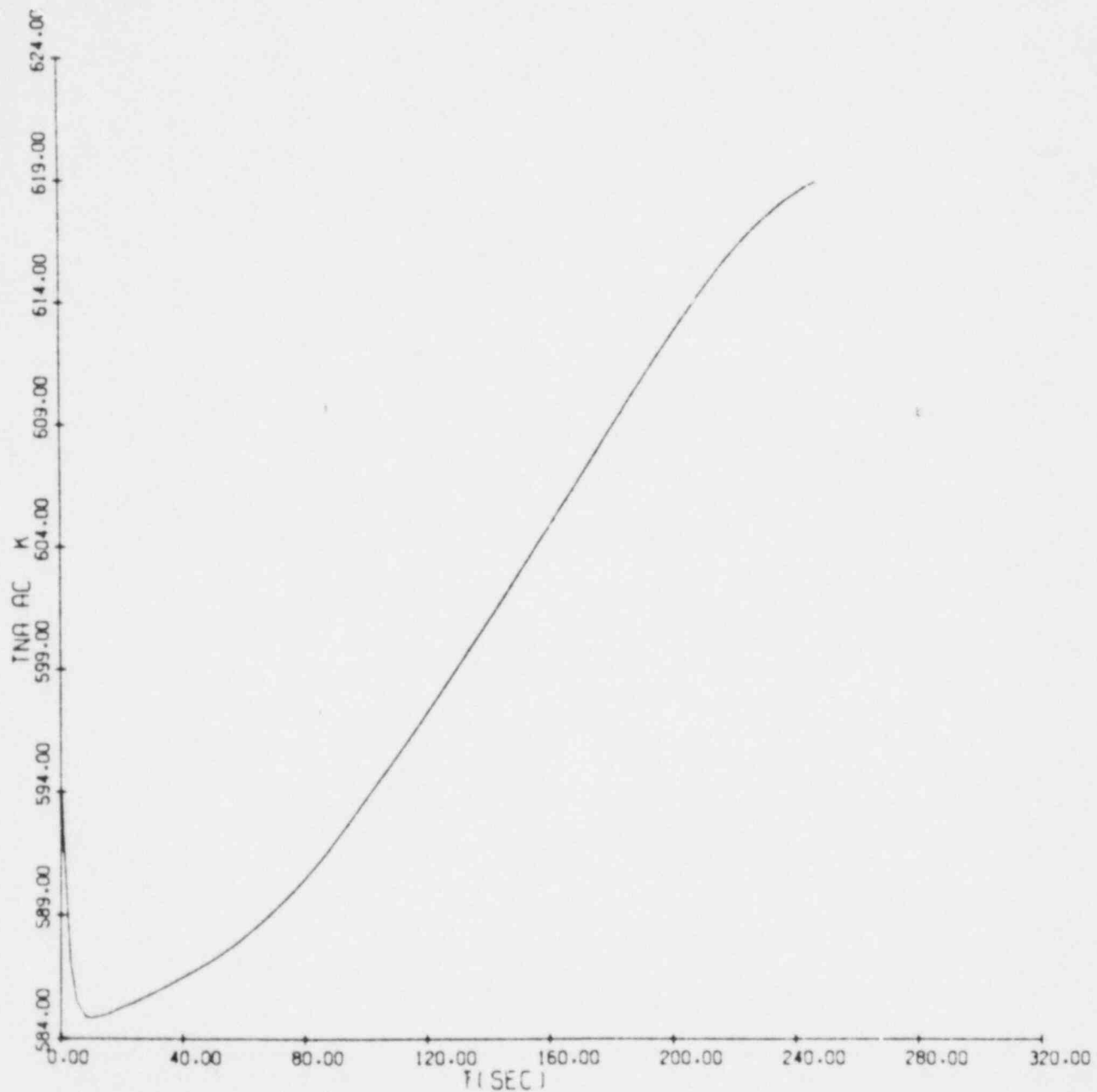


Figure 17: Nominal DEMO-F prediction of the core exit temperature for the average channel for the 5% LOP test in FFTF assuming 25 hours of prior operation at 5% power.

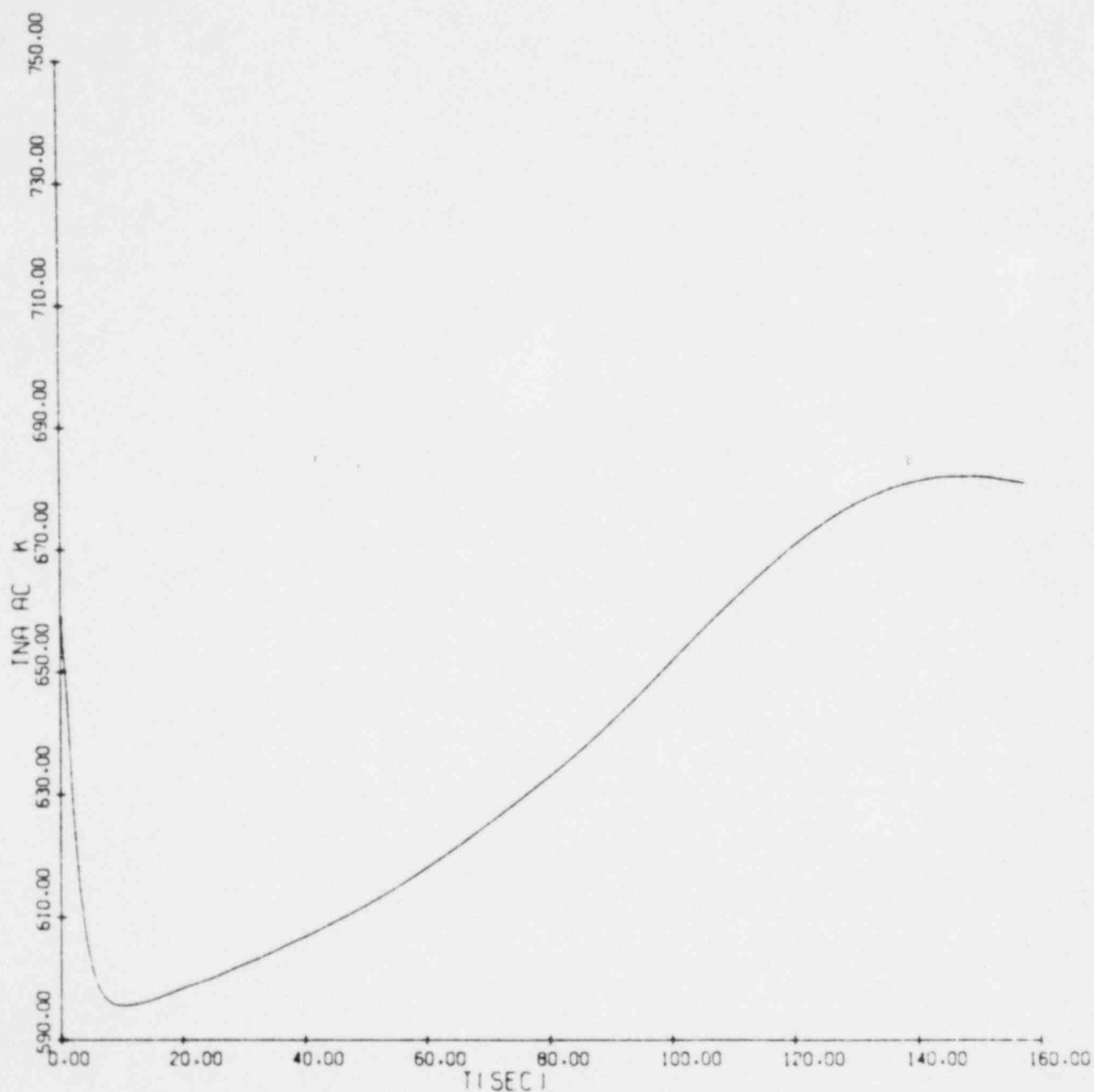


Figure 18: Nominal DEMO-F prediction of the core exit temperature for the average channel for the 35% LOP test in FFTF assuming 25 hours of prior operation at 35% power.

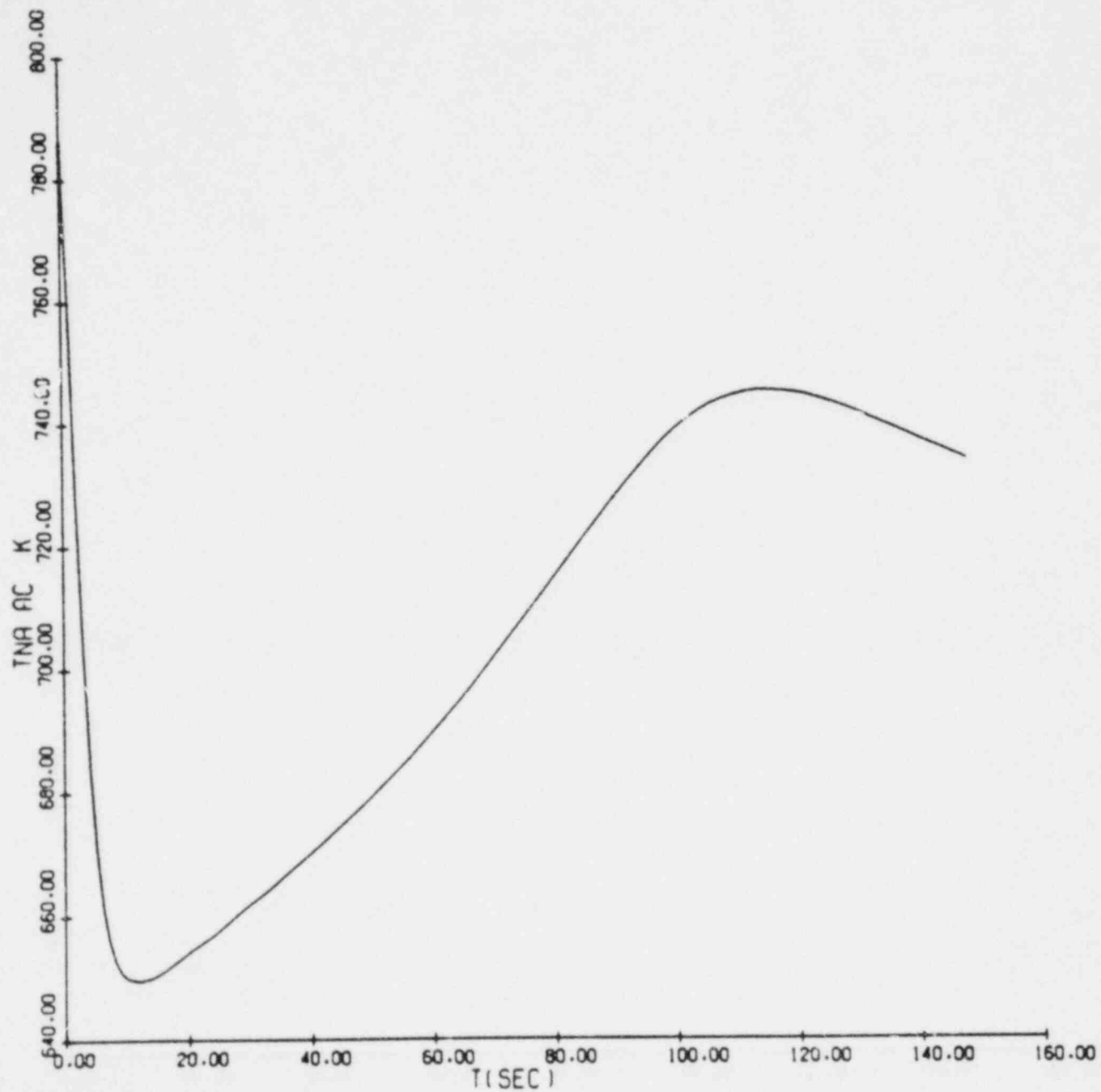


Figure 19: Nominal DEMO-F prediction of the core exit temperature for the average channel for the 75% LOP test in FFTF assuming 25 hours of prior operation at 75% power.

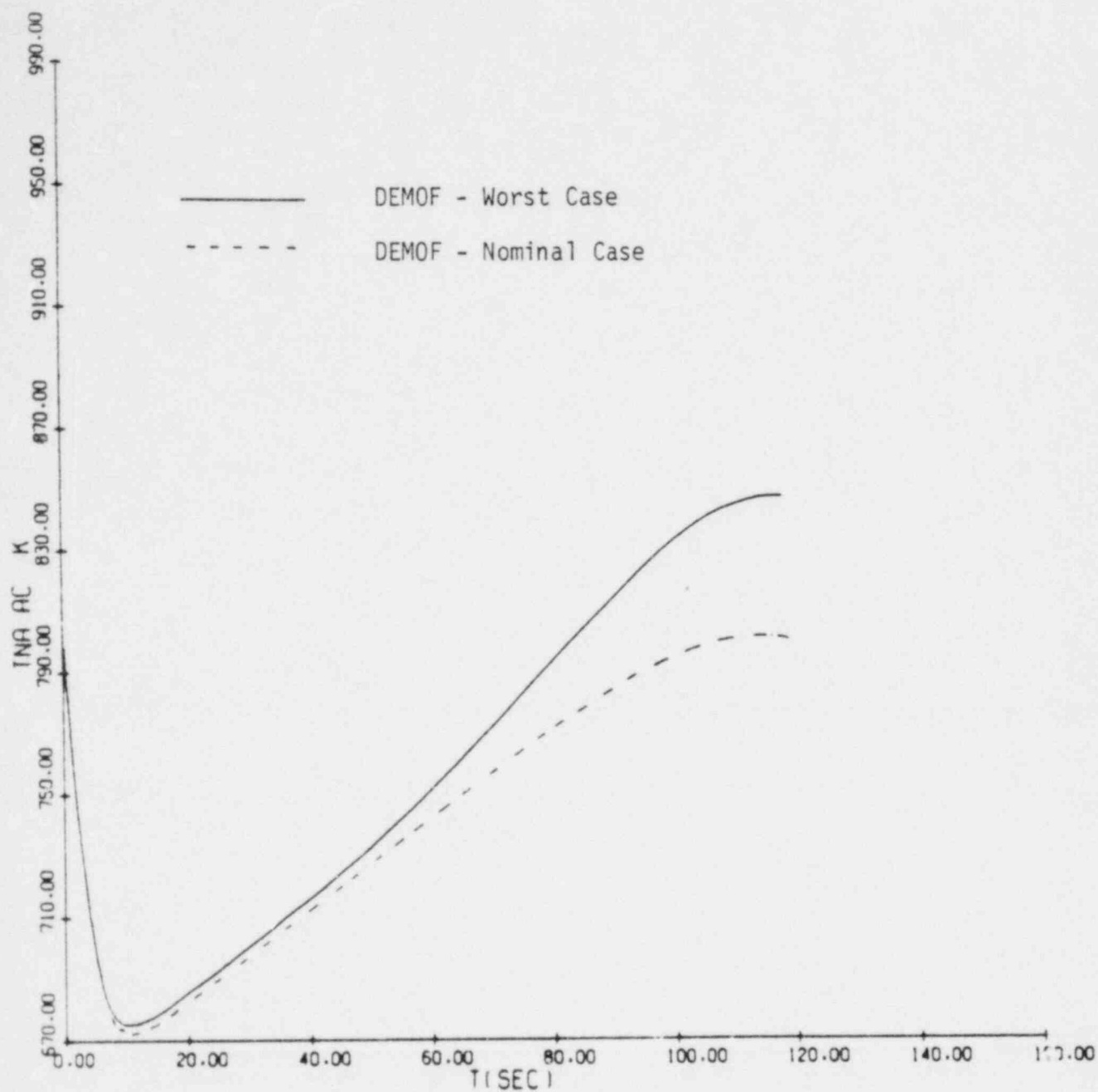


Figure 20: Nominal and worst case DEMO-F prediction of the core exit temperature for the average channel for the 100% LOP test in FFTF assuming 25 hours of prior operation at 100% power.

As previously indicated, the margin between the nominal FLODISC prediction and that used in IANUS is nonexistent for steady-state conditions. Therefore, the verification of the conservatism inherent in the FLODISC calculation will rely heavily on the transient natural circulation tests. The predictions for the 100% test using the various models are summarized in Table 5. Note that the average FOTA  $\Delta T$  is used in preference to the maximum FOTA  $\Delta T$  because FLODISC does not realistically model intra-subassembly flow redistribution. In regions where there is a steep power gradient (e.g., the row 6 FOTA), FLODISC is expected to be very conservative (since it does not model crossflow or conduction between channels), but this is almost irrelevant for verification of the statistical hot-channel where the power gradient is assumed to be flat. The predicted hot-channel  $\Delta T$  has been included in Table 5 for the purpose of benchmarking differences between the Project's calculations and the present calculations. It is hoped that this will aid in establishing continuity between the analyses used to support the FSAR and the ongoing verification program.

There are several features of the predictions summarized in Table 5 which bear some elaboration. First, it may be noticed that there is good agreement between HEDL's IANUS predictions and the present nominal IANUS predictions. This does not mean that all features of the modeling are identical. It only means that most of the differences (if there are any), "wash out" by the time the peak in temperature occurs. The few degrees difference in the results are probably due to the present use of nominal pipe and pump stopped rotor pressure drop (instead of the conservative default values). Some details of the models (pump trip time, reactivity insertion, etc.) will have important consequence on the short-term behavior but will have all but disappeared by the time transition to natural circulation occurs. Specifically, the gap conductance of fresh fuel is likely to be much lower (particularly at low power levels) than the default value which is characteristic of highly irradiated fuel. A low gap conductance increases stored energy in the fuel rods and affects the initial cool-down as seen in Figure 21, but after about 20 seconds there is no appreciable difference in the calculation.

It is also worthy of note that the first three columns of Table 5 are given for purposes of illustration and cannot be directly verified. The

Table 5

Comparison of Nominal and Worst Case Predictions  
of Maximum Temperatures for the FFTF 100% LOP  
Test After 25 Hours of Full Power Operation

	Average Assembly Outlet Temperature (K)	Hot Channel $\Delta T$ (K)	Core $\Delta T$ (Without Bypass) (K)	Average Row 2 FOTA $\Delta T$ (K)	Average Row 6 FOTA $\Delta T$ (K)
IANUS Nominal	796	246	162	-	-
IANUS Worst Case	835	305	200	-	-
DEMO-F Nominal	793	240	159	-	-
DEMO-F Worst Case	845	255	210	-	-
FLODISC <sup>(1)</sup> Nominal	764	235	130	140	125
FLODISC <sup>(1)</sup> Worst Case	767	260	133	165	160
FLODISC <sup>(1)</sup> Steady-State	785	246	151	159	145
HEDL FLODISC	798	232	164	N/A <sup>(2)</sup>	N/A <sup>(2)</sup>
HEDL IANUS	800	252	165	N/A <sup>(2)</sup>	N/A <sup>(2)</sup>

(1) Based on nominal core flow predictions and accounting for redistribution from bypass to core.

(2) N/A - Not presently available.

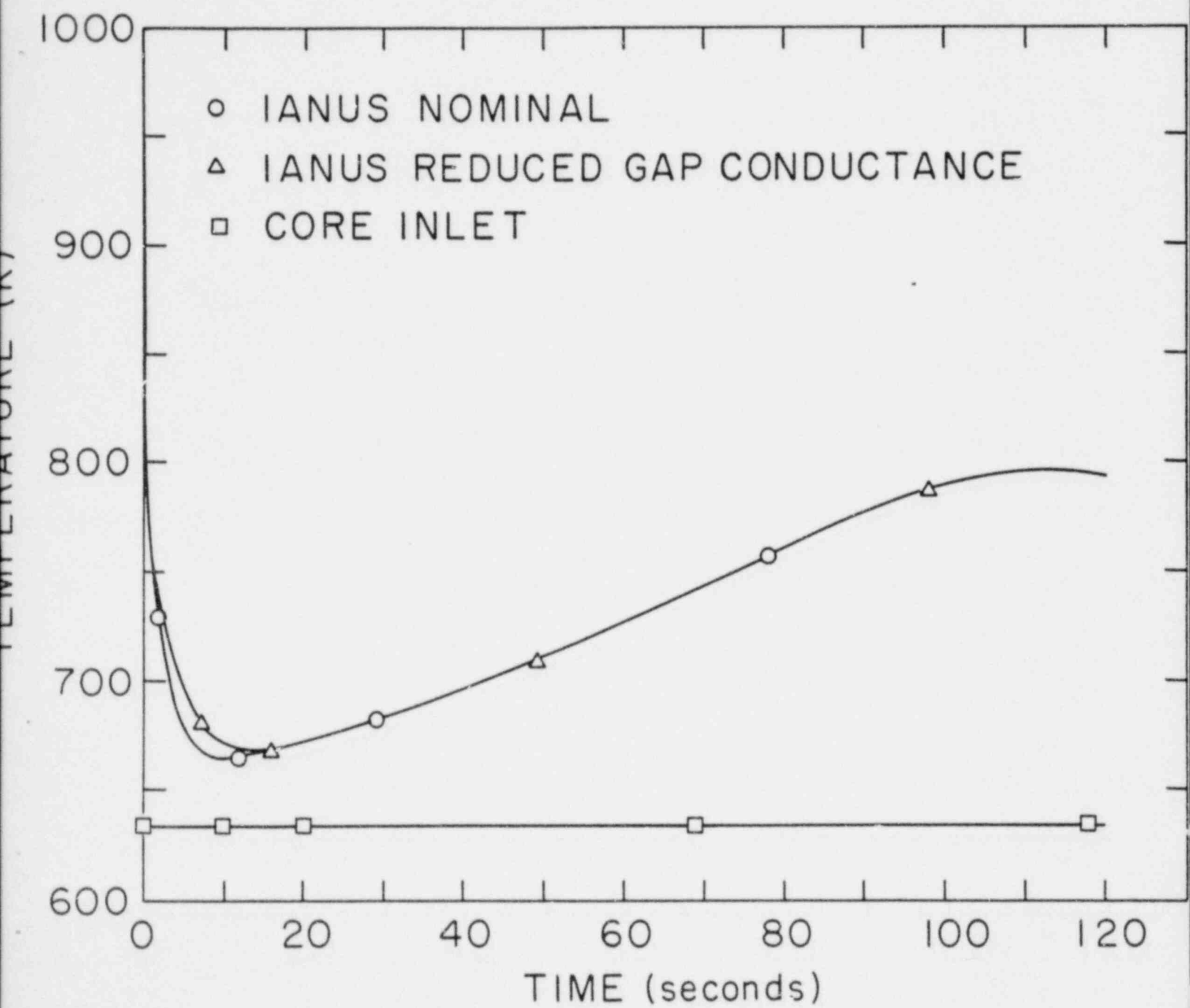


Figure 21: Nominal IANUS prediction of the core exit temperature for the 100% LOP test compared to the identical prediction using limiting gap conductance.

core  $\Delta T$  and resulting outlet temperature are effectively flow-weighted averages of all assemblies and will be difficult to interpret during the transient. The hot-channel  $\Delta T$  is a worst case combination of variables and cannot be measured directly. Thus, verification of transient core temperature predictions will rely on the FLODISC predictions of FOTA  $\Delta T$ 's and/or FOTA flow rates. The FOTA  $\Delta T$ 's have been used for illustration since they are expected to be more accurate, but this will depend on the final resolution of measurement uncertainties.

The most significant feature of Table 5 is the radical difference between the FLODISC calculations. This difference shows up most dramatically in the core  $\Delta T$  predictions. The BNL predictions of core  $\Delta T$  range from 130 to 151 K while the FFTF Project predicts 164 K. This inconsistency in the predictions can be attributed to the difference in core models. The FFTF Project used a nine channel model of the core which did not include the bypass region. This treatment precludes redistribution from the bypass regions, a factor which greatly affects the overall prediction. The present FLODISC predictions used essentially the same 12 channel model which had been submitted in support of the flow dependent hot-channel factors with slight modifications to the flow and power of channels 2 and 7 to represent the FOTAs. Thus, redistribution from the unheated bypass regions causes the predicted core  $\Delta T$  to be substantially lower than the IANUS calculation (with a fixed flow fraction). It should be made clear that while IANUS assumes a constant flow split (resulting in a relatively high core  $\Delta T$ ), the hot-channel factor is based on flow redistribution calculation and in that respect is inconsistent with the core  $\Delta T$  calculation.

It is clear from Table 5, that there is a great diversity of predictions to be verified by the test program. The present nominal test predictions are much less conservative than the Project's test predictions, but the present calculations appear to be more consistent with the previous safety analyses.<sup>(1,7,8,9,20)</sup> This consistency seems to be necessary if the verification program is to have any relevance to the previous safety analyses.

HEDL has recently provided<sup>(22)</sup> more detailed test predictions for the 5% transient test. In this case, HEDL has used CORA<sup>(23)</sup> instead of FLODISC<sup>(5)</sup> to make individual subassembly calculations. Comparisons between the present

predictions\* and the HEDL predictions are summarized in Table 6. Note that in this case the agreement between HEDL and BNL calculations is quite good but it is not clear whether this is due to a change in the HEDL model (from FLODISC to CORA) or due to the lack of beneficial flow redistribution at these extremely low flow rates. (For the 5% test the minimum Reynolds number in the test assemblies is predicted to be 500 and the tendency toward beneficial flow redistribution is negated by the relatively high frictional resistance of the fueled assemblies.) Without this beneficial redistribution, the active core  $\Delta T$  predicted by DEMO and IANUS becomes nearly equal to the average core  $\Delta T$  predicted by FLODISC (57 K).

A recent change (transmitted informally) to the 35% power test will make it a valuable tool in verifying unbalanced loop performance. Present plans call for leaving one secondary pony motor on while the others are shut down. This changes the thermal center of the affected IHX and causes the natural circulation in the affected primary loop to be substantially higher than that in the remaining two loops. Such flow imbalance is characteristic of the "contrived" earthquake and tornado events<sup>(8)</sup> which lead to boiling in the core. While the predicted flow imbalance (shown in Figure 22) is not as substantial as the imbalance predicted for some of the "contrived" cases (where negative loop flow can occur), the predicted flow in the affected loop is 30% greater than the unaffected loops. This difference in loop flow may be severe enough to demonstrate whether unbalanced loop flow can produce asymmetric flow in the core (a possibility which is not accounted for by either FLODISC or CORA). In any case, this unbalanced test should provide valuable data for validating the transient IHX performance.

The BNL predictions for the 35% test are summarized in Table 7. The corresponding HEDL predictions are not yet available. Note that the unbalanced loop configuration has very little effect on the core temperatures in that the predicted temperatures would only be 4 to 6 K higher for a balanced loss-of-power test (not shown). The FOTA temperature data for the 35% test can be

---

\*As of the report date, the 5% test has been run but the term "predictions" is still used since the results are not yet available.

TABLE 6

Comparison Between HEDL and BNL Nominal Predictions for  
the 5 Percent Loss-of-Power Test in FFTF After One Hour  
of Prior Operation at 5 Percent Power

	HEDL CALCULATION USING CORA	BNL CALCULATION USING FLODISC
Peak Row 2 FOTA Coolant Temperatures at Top of Fuel (K).	616.8	617.6
Peak Row 6 FOTA Coolant Temperatures at Top of Fuel (K).	609.5	611.5
Minimum Flow Rate for Row 2 FOTA (% of initial).	0.52	0.41
Minimum Flow Rate for Row 6 FOTA (% of initial).	0.50	0.44

# PLANT FLOW RATES

NAT CIRC ON PRIMARY LOOP 35% POWER 75% FLOW

CASE NUMBER 3040

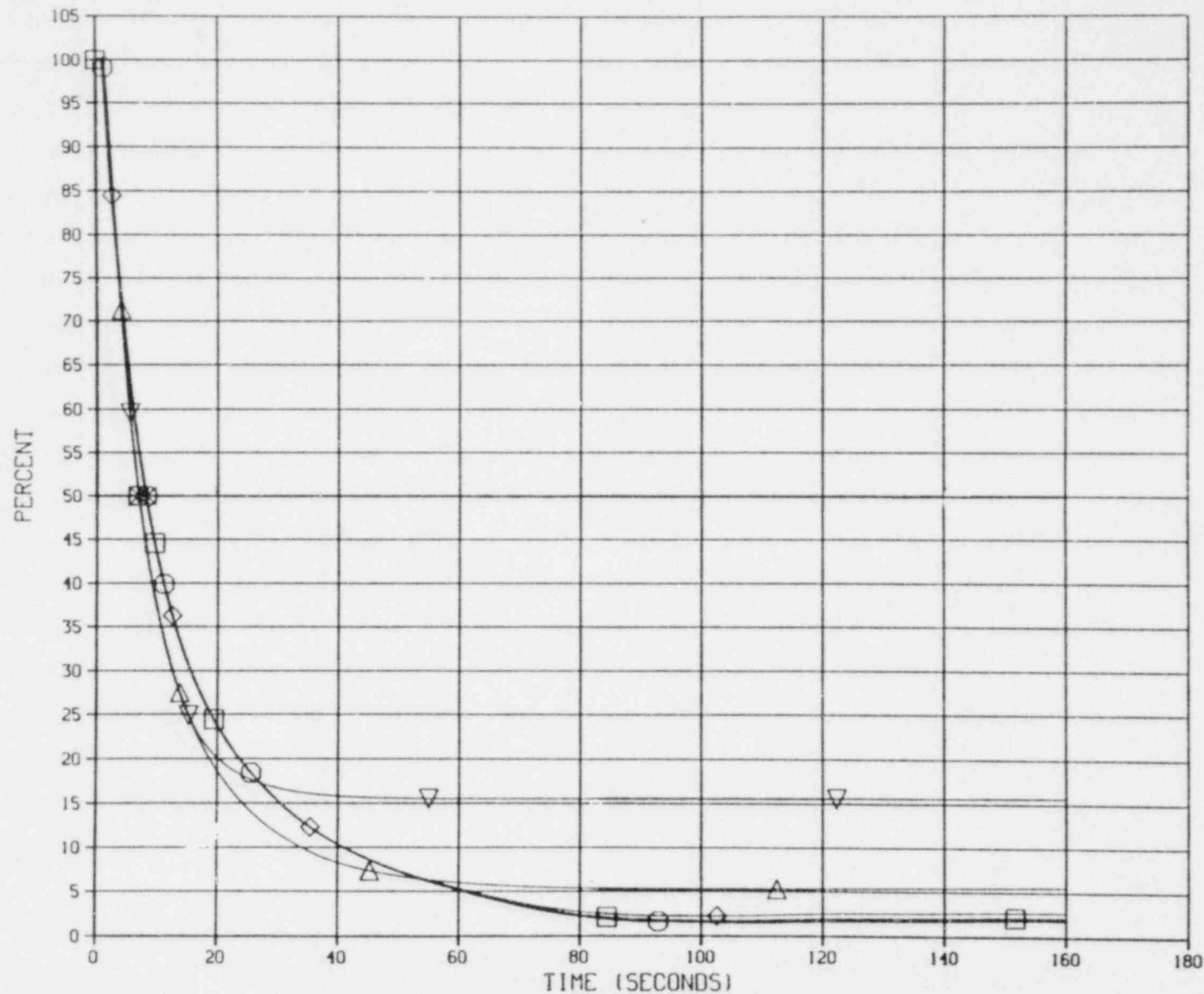


Figure 22: Primary and secondary flow rates for the 35% unbalanced LOP test in FFTF assuming 25 hours of prior operation at 35% power.

TABLE 7

Summary of BNL Test Predictions of the Maximum Temperatures  
for the 35% Unbalanced Loop Loss-of-Power Test in FFTF

	AVERAGE ASSEMBLY OUTLET TEMP. (K)	AVERAGE CORE $\Delta T$ (WITHOUT BYPASS) (K)	ROW 2 FOTA $\Delta T$ (K)	ROW 6 FOTA $\Delta T$ (K)
IANUS-Nominal after 1 hr Operation	648	64	-	-
IANUS-Nominal after 25 hrs Operation	675	91	-	-
DEMO-Nominal after 25 hrs Operation	677	92	-	-
FLODISC(1) Nominal	640	57	64	55
FLODISC(1) Worst Case	642	59	76	66

(1) Based on nominal core flow predictions for one hour operation  
and accounting for redistribution from bypass to core.

expected to provide important validation of inherent natural circulation capability before progressing to tests at higher power levels. Relative differences in loop behavior will also help to characterize the IHX under off design conditions. The flow rates for the I-loop (representing the two unaffected loops) and the P-loop (representing the one loop with the secondary pony motor still on) are shown in Figure 22. The predicted IHX outlet temperatures for the primary loops are shown in Figure 23 and for the secondary loops are shown in Figure 24.

### 3.2.3 Uncertainty Analyses

A thorough analysis of measurement uncertainty appears to be needed if the verification program is to succeed in identifying the capabilities and deficiencies in the codes. Nominal and worst case models of the plant have been used to anticipate the range of behavior. The computer codes used for these predictions attempt to model the important phenomena affecting performance during the LOP event. However, it should be recognized that several unmodeled effects have been identified which may have significant effects for some of the postulated events. Special tests and measurements have been identified which will aid in establishing the significance of these unmodeled effects, but as with the rest of the test program, it will be important to compare the measurement accuracy to the range of anticipated behavior.

# IHX TEMPERATURES - P LOOP

## NAT CIRC ON PRIMARY LOOP 35% POWER 75% FLOW

CASE NUMBER 3040

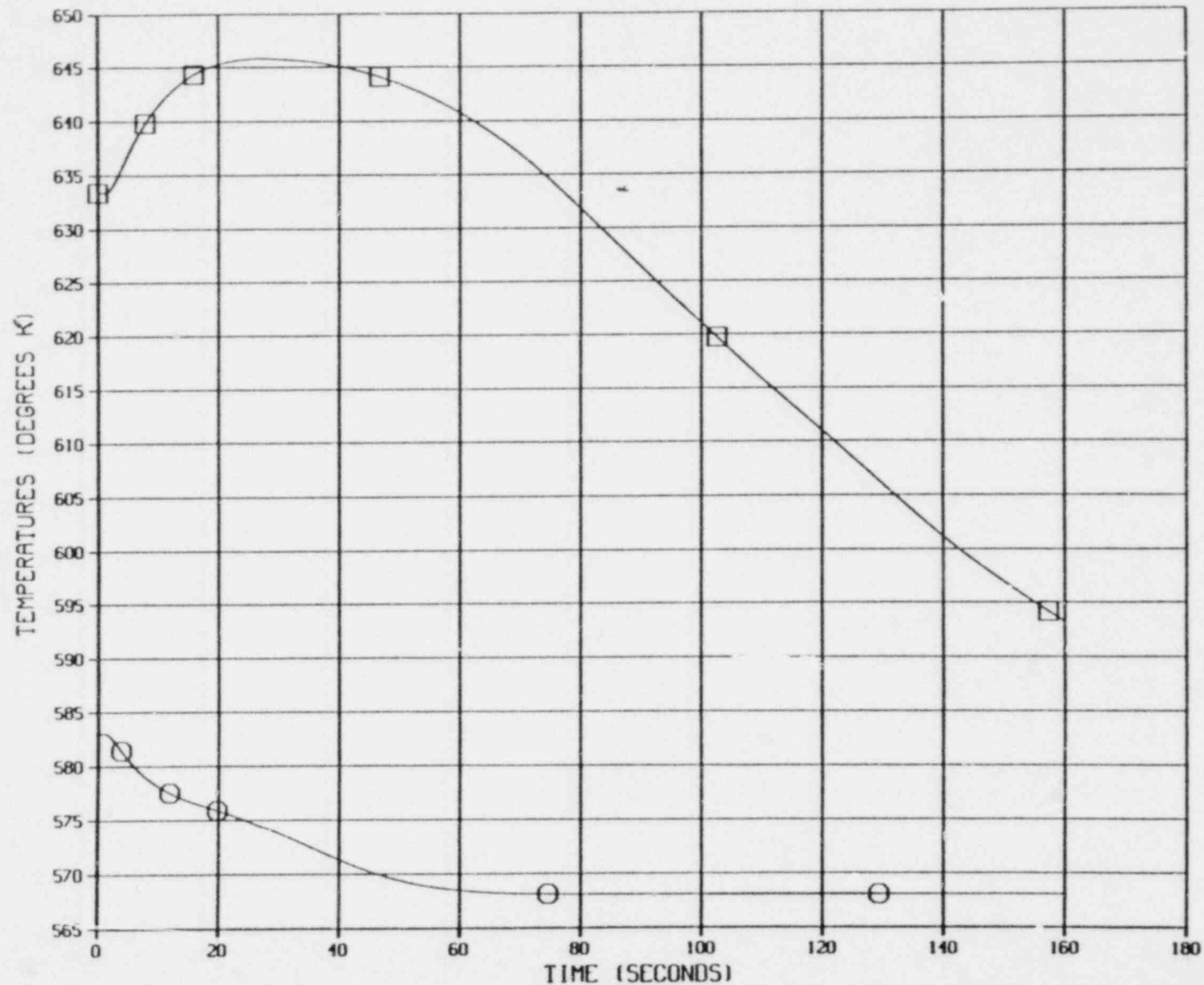


Figure 23: Primary and secondary IHX outlet temperatures for the P-loop (representing 3 loops with pony motors off) during the 35% unbalanced LOP test in FFTF assuming 25 hours of prior operation at 35% power.

# IHX TEMPERATURES - I LOOP

NAT CIRC ON PRIMARY LOOP 35% POWER 75% FLOW

CASE NUMBER 3040

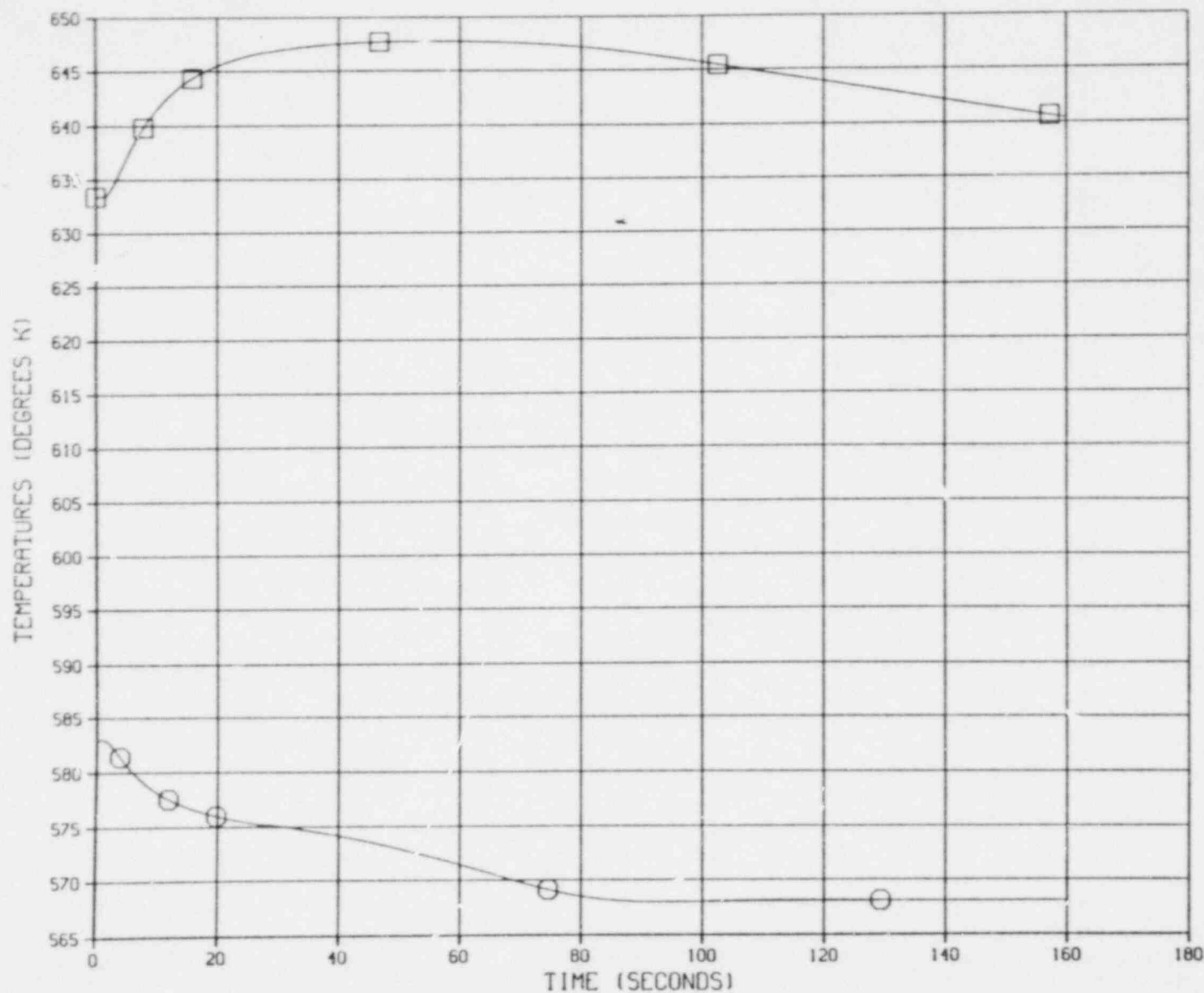


Figure 24: Primary and secondary IHX outlet temperatures for the I-loop (representing the 1 loop with a secondary pony motor running) during the 35% unbalanced LOP test in FFTF assuming 25 hours of prior operation at 35% power.

#### 4.0 SUMMARY AND CONCLUSIONS

DEMO-F, IANUS, and FLODISC have been used at Brookhaven to analyze the preliminary results of the FFTF natural circulation tests and to make predictions of the primary test series scheduled after the core is loaded. The comparisons of the BNL analysis with the data and previous HEDL calculations indicated that:

(1) There is generally good agreement with nominal modeling for the steady-state tests.

(2) The BNL IANUS transient calculations followed the data trends, but were inaccurate in several respects, as discussed below.

(3) The pump coastdown model tended to underpredict secondary flow rate, but it has very little effect on the thermal transient for the secondary tests.

(4) BNL and HEDL calculations show substantial differences although they employ superficially identical modeling.

(5) The calculated results are very sensitive to the measured heat losses which appear to be dominated by air infiltration through leakage paths. Some assessment needs to be made of the accuracy of these measurements and of whether the heat losses can change with time (i.e., whether dampers can become misaligned with usage).

The generally good agreement of the data with the steady-state tests is reassuring with respect to predictive capability, but careful analysis of experimental uncertainties needs to be performed in order to evaluate the uncertainty interval and/or the confidence level associated with the conservative (worst case) models. This is particularly true at low flow rates where the data tends toward agreement with the worst case models.

The main reason for inaccuracies in the IANUS transient thermal calculations appears to be due to the fixed number<sup>(7)</sup> of nodes in the DHX along with modeling more suitable to a counterflow heat exchanger. The FFTF actually has a four-pass, cross-flow dump heat exchanger. The errors in the transient prediction can be substantially reduced by changing to a more appropriate nodalization. Even with improved modeling in the DHX (e.g., using air temperatures representative of a four-pass cross flow heat exchanger), the flow response to

the thermal transient in the cold leg appears to be somewhat more rapid than the data indicate. These errors in response time are probably due to a combination of effects including: coarse nodalization in the DHX and cold leg; neglecting thermal capacity of the outlet manifold, pump, and pump tank volumes; differences in pipe lengths from the various modules; stratification in various cold leg segments; and fictitious energy transport via numerical mixing (NMIX).

While it is clear that more detailed data comparisons (e.g., temperature at the pump and IHX inlet) are needed to determine which of these effects dominate the transient behavior, the severity of the thermal transient is a direct result of the mismatch in thermal capacity between the air and sodium sides of the DHX. This mismatch is not nearly as severe for the primary system (with a sodium-to-sodium heat exchanger). Although the LOP from refueling conditions is interesting for code validation (since it provides a good test of modeling capability), the predictive capability (or lack thereof) has limited safety implications. That is, the LOP from refueling conditions is essentially a demonstration test (for this event) and limited success in modeling the details of the DHX performance has very little impact on the initial response of the reactor core for the hypothetical LOP from full power event (due to the large transport times involved).

The differences between the Brookhaven and HEDL calculations for both the primary and secondary tests point out the need for complete documentation of the models to be verified and their relation to the models used in previous safety analyses. The differences in modeling detail are highlighted by the comparisons to the data for the LOP from refueling conditions. The default IANUS model of the DHX demonstrated good qualitative agreement with the data and required only a more realistic air temperature distribution (characteristic of the actual four-pass, cross-flow heat exchanger rather than the seven-pass model employed) to obtain reasonably good agreement with the non-linear performance characteristic of the unbalanced DHX.

## REFERENCES

1. "FFTF Final Safety Analysis Report", HEDL-TI-75001, (December 1975).
2. U.S. Nuclear Regulatory Commission, "FFTF Safety Evaluation Report", NUREG-0358, (August 1978).
3. HEDL, "Interim Summary of FFTF Natural Circulation Test Plans", submitted to DPM/NRC for review, (September 1977).
4. S.L. Additon, T.B. McCall and C.F. Wolfe, "Simulation of the Overall FFTF Plant Performance", HEDL TC-556, (March 1976).
5. J. Muraoka et al., "FLODISC - A Dynamic Core Flow Distribution Code: Evaluation of the Total Loss of Electrical Power Event", HEDL-TC-874, (May 1977).
6. T.R. Beaver, "Evaluation of Secondary HTS Transient Natural Circulation Test", interim report submitted to NRC for review, (June 1979).
7. S.L. Additon, A.E. Strait and C.F. Wolfe, "FFTF Natural Circulation Evaluation: Transition to Natural Circulation", HEDL-TC-557, (April 1976).
8. S.L. Additon, E.A. Parziale and C.F. Wolfe, "FFTF Decay Heat Removal Analysis: Effects of Natural Phenomena", HEDL-TI-75222, (October 1976).
9. K.R. Perkins, R.A. Bari, L.C. Chen and D.C. Albright, "Analyses of FFTF System Transients", Informal Report, BNL-NUREG-25560, (January 1979).
10. R.R. Lowrie and W.J. Severson, "A Preliminary Evaluation of the CRBRP Natural Circulation Decay Heat Removal Capability", WARD-D-0132, (March 1976).
11. K.R. Perkins, R.A. Bari and D.C. Albright, "Uncertainties in the Calculated Response of the Clinch River Breeder Reactor During Natural Circulation Decay Heat Removal", Informal Report, BNL-NUREG-22715, (April 1977).
12. Westinghouse, ARD, "LMFBR Demo Plant Simulation Model (DEMO)", Rev. 4, WARD-D-0005, (January, 1976).

13. Amendment 32 of the "CRBRP Preliminary Safety Analysis Report", Project Management Corporation, (docketed June 1975).
14. H. Domanus, R.C. Schmitt and W.T. Shaw, "Numerical Results Obtained from the Three-Dimensional, Transient, Single-Phase Version of the COMMIX Code", NUREG-0355, (October 1977).
15. K.E. Kasza, R.D. Schmitt and W.T. Sha, "Thermal Buoyancy Phenomena in a Horizontal Pipe During a Flow Coastdown Thermal-Hydraulic Transient", ANS-CT-77-31, (September 1977).
16. K.E. Kasza, M.M. Chen and M.J. Binder, "Initial Considerations on the Influence of Thermal Buoyancy on Heat Exchanger Performance", Technical Memorandum, ANL-CT-47, (August 1978).
17. S.L. Additon, "Presentation to the Advisory Committee on Reactor Safety", (November 1977).
18. D.M. Turner, "Pretest Predictions for HTS Secondary Transient Natural Circulation Test", submitted to NRC/RSB for review, (May 1979).
19. A.Z. Frangos, "FFTF HTS/DHX Prototype Module Testing in SCTI, Final Report", LMEC-76-4, (October 1976).
20. S.L. Additon, P.A. Edwards and W.L. Knecht, "FFTF Long Term Natural Circulation Decay Heat Removal Analysis", HEDL-TC-598, (April 1976).
21. K.R. Perkins and R.A. Bari, "Interassembly Flow Redistribution at Natural Circulation Conditions in the Fast Flux Test Facility", Trans. Am. Nucl. Soc., 30, 413 (November 1978).
22. H.G. Johnson, "Pretest Predictions of the Thermal and Hydraulic Responses of the Fueled Open Test Assemblies to the 5 Percent Power Natural Circulation FFTF Plant Startup Test", HEDL-TC-1778, (August 1980).
23. H.G. Johnson, "CORA - A Computer Code for Thermal and Hydraulic Coupling of Reactor Core Assemblies", HEDL-TC-1505, (September 1979).



DISTRIBUTION LIST

Dr. Raymond Alcouffe Los Alamos Scientific Laboratory Mail Stop 269 P. O. Box 1663 Los Alamos, New Mexico 87545	(1)
Mr. Harry Alter, Chief NE 563 RRT Division Department of Energy Washington, D. C. 20545	(1)
Dr. Robert Avery, Director Reactor Analysis & Safety Division Argonne National Laboratory 9700 South Cass Avenue Argonne, IL 60439	(2)
Mr. Marshall Berman Sandia Laboratories P. O. Box 5800 Albuquerque, New Mexico 87115	(1)
Mr. Robert M. Bernero, Director Division of Systems & Reliability Research Office of Nuclear Regulatory Research U. S. Nuclear Regulatory Commission Washington, D. C. 20555	(1)
Mr. Walter R. Butler, Chief Containment Systems Branch Division of Systems Integration Office of Nuclear Reactor Regulation U. S. Nuclear Regulatory Commission Washington, D. C. 20555	(1)
Dr. L. W. Caffey, Director CRBR Plant Project Office Department of Energy P. O. Box U Oak Ridge, TN 37830	(1)
Dr. Ivan Catton University of California at Los Angeles Los Angeles, California 90024	(1)

Central Mail & Files (2)  
U. S. Nuclear Regulatory Commission  
Public Document Room (LMFBR)  
Washington, D. C. 20555

Mr. Paul S. Check, Assistant Director (1)  
for Plant Systems  
Division of Systems Integration  
Office of Nuclear Reactor Regulation  
U. S. Nuclear Regulatory Commission  
Washington, D. C. 20555

Dr. Robert T. Curtis, Chief (1)  
Analytical Advanced Safety Technology Branch  
Division of Reactor Safety Research  
Office of Nuclear Regulatory Research  
U. S. Nuclear Regulatory Commission  
Washington, D. C. 20555

Dr. William Davey (1)  
Q Division Leader  
Mail Stop 561  
Los Alamos Scientific Laboratory  
P. O. Box 1663  
Los Alamos, NM 87545

Mr. Harold R. Denton, Director (1)  
Office of Nuclear Reactor Regulation  
U. S. Nuclear Regulatory Commission  
Washington, D. C. 20555

Director (1)  
Division of Reactor Safety Research  
Office of Nuclear Regulatory Research  
U. S. Nuclear Regulatory Commission  
Washington, D. C. 20555

Director (1)  
Fast Flux Test Facility Project Office  
Department of Energy  
P. O. Box 550  
Richland, WA 99352

Dr. Raymond DiSalvo, Chief (1)  
Operational Safety Research Branch  
Division of Reactor Safety Research  
Office of Nuclear Regulatory Research  
U. S. Nuclear Regulatory Commission  
Washington, D. C. 20555

Mr. Darrell G. Eisenhut, Director (1)  
Division of Licensing  
Office of Nuclear Reactor Regulation  
U. S. Nuclear Regulatory Commission  
Washington, D. C. 20555

Mr. Malcolm L. Ernst, Assistant Director (1)  
for Technology  
Division of Safety Technology  
Office of Nuclear Reactor Regulation  
U. S. Nuclear Regulatory Commission  
Washington, D. C. 20555

Mr. Frank Gavigan (1)  
NE 563  
RRT Division  
Department of Energy  
Washington, D. C. 20545

Mr. Stephen S. Hanauer, Director (1)  
Division of Human Factors Safety  
Office of Nuclear Reactor Regulation  
U. S. Nuclear Regulatory Commission  
Washington, D. C. 20555

Mr. Robert W. Houston, Chief (1)  
Accident Evaluation Branch  
Division of Systems Integration  
Office of Nuclear Reactor Regulation  
U. S. Nuclear Regulatory Commission  
Washington, D. C. 20555

Dr. Harry Hummel (1)  
Applied Physics Division  
Argonne National Laboratory  
Building 208  
9700 South Cass Avenue  
Argonne, IL 60439

Mr. William V. Johnston, Chief (1)  
Core Performance Branch  
Division of Systems Integration  
Office of Nuclear Reactor Regulation  
U. S. Nuclear Regulatory Commission  
Washington, D. C. 20555

Dr. William Kastenbergl  
Department of Chemical, Nuclear  
and Thermal Engineering  
University of California  
at Los Angeles  
Los Angeles, California 90024 (1)

Dr. Charles N. Kelher, Assistant Director  
for Advanced Reactor Safety Research  
Division of Reactor Safety Research  
Office of Nuclear Regulatory Research  
U. S. Nuclear Regulatory Commission  
Washington, D. C. 20555 (1)

Mr. George W. Knighton, Chief  
Research & Standards Coordination Branch  
Division of Safety Technology  
Office of Nuclear Reactor Regulation  
U. S. Nuclear Regulatory Commission  
Washington, D. C. 20555 (1)

Mr. William E. Kreger, Assistant Director  
for Radiation Protection  
Division of Systems Integration  
Office of Nuclear Reactor Regulation  
U. S. Nuclear Regulatory Commission  
Washington, D. C. 20555 (1)

Manager, Safety Engineering  
Hanford Engineering Development  
Laboratory  
P. O. Box 1970  
Richland, WA 99352 (1)

Dr. James F. Meyer  
Reactor Systems Branch  
Division of Systems Integration  
Office of Nuclear Reactor Regulation  
U. S. Nuclear Regulatory Commission  
Washington, D. C. 20555 (15)

Mr. Warren Minners, Technical Assistant  
Division of Safety Technology  
Office of Nuclear Reactor Regulation  
U. S. Nuclear Regulatory Commission  
Washington, D. C. 20555 (1)

Dr. Robert Minoque, Director  
Office of Nuclear Regulatory Research  
U. S. Nuclear Regulatory Commission  
Washington, D. C. 20555 (1)

Mr. Thomas Murley, Director (1)  
Division of Safety Technology  
Office of Nuclear Reactor Regulation  
U. S. Nuclear Regulatory Commission  
Washington, D. C. 20555

Mr. Thomas M. Novak, Assistant Director (1)  
for Operating Reactors  
Division of Licensing  
Office of Nuclear Reactor Regulation  
U. S. Nuclear Regulatory Commission  
Washington, D. C. 20555

Dr. David Okrent (1)  
Department of Chemical, Nuclear and  
Thermal Engineering  
University of California  
at Los Angeles  
Los Angeles, California 90024

Mr. Denwood F. Ross, Director (1)  
Division of Systems Integration  
Office of Nuclear Reactor Regulation  
U. S. Nuclear Regulatory Commission  
Washington, D. C. 20555

Mr. Francis H. Rowsome, Acting Chief (1)  
Systems Analysis Branch  
Division of Systems & Reliability Research  
Office of Nuclear Regulatory Research  
U. S. Nuclear Regulatory Commission  
Washington, D. C. 20555

Mr. Lester S. Rubenstein, Assistant Director (1)  
for Reactor Systems  
Division of Systems Integration  
Office of Nuclear Reactor Regulation  
U. S. Nuclear Regulatory Commission  
Washington, D. C. 20555

Mr. Frank Schroeder, Assistant Director (1)  
for Generic Projects  
Division of Safety Technology  
Office of Nuclear Reactor Regulation  
U. S. Nuclear Regulatory Commission  
Washington, D. C. 20555

Secretary, Advisory Committee on (5)  
Reactor Safeguards  
U. S. Nuclear Regulatory Commission  
Washington, D. C. 20555

Mr. Melvin Silberberg, Chief Experimental Safety Technology Branch Division of Reactor Safety Research Office of Nuclear Regulatory Research U. S. Nuclear Regulatory Commission Washington, D. C. 20555	(1)
Dr. Themis P. Speis, Chief Reactor Systems Branch Division of Systems Integration Office of Nuclear Reactor Regulation U. S. Nuclear Regulatory Commission Washington, D. C. 20555	(1)
Mr. Victor Stello, Director Office of Inspection & Enforcement U. S. Nuclear Regulatory Commission Washington, D. C. 20555	(1)
Dr. Michael Stevenson Los Alamos Scientific Laboratory P. O. Box 1663 Los Alamos, NM 87545	(2)
Mr. John F. Stolz, Chief Systems Interaction Branch Division of Systems Integration Office of Nuclear Reactor Regulation U. S. Nuclear Regulatory Commission Washington, D. C. 20555	(1)
Dr. David G. Swanson Applied Science Associates, Inc. P. O. Box 214 Hawthorne, California 90250	(1)
Technical Information Center U. S. Nuclear Regulatory Commission P. O. Box 62 Oak Ridge, TN 37830	(2)
Mr. Ashok Thadani, Chief Reliability & Risk Assessment Branch Division of Safety Technology Office of Nuclear Reactor Regulation U. S. Nuclear Regulatory Commission Washington, D. C. 20555	(1)
Dr. Theo G. Theofanous 132 Pathway Lane Lafayette, Indiana 47906	(1)

Dr. Long Sun Tong, Chief Scientist (1)  
Assistant Director for Water Reactor  
Safety Research  
Division of Reactor Safety Research  
U. S. Nuclear Regulatory Commission  
Washington, D. C. 20555

Mr. Steven A. Varga, Chief (1)  
Operating Reactors Branch No. 1  
Division of Licensing  
Office of Nuclear Reactor Regulation  
U. S. Nuclear Regulatory Commission  
Washington, D. C. 20555

Mr. Richard H. Vollmer, Director (1)  
Division of Engineering  
Office of Nuclear Reactor Regulation  
U. S. Nuclear Regulatory Commission  
Washington, D. C. 20555

Dr. J. V. Walker, Dept. Manager (1)  
Reactor Research and Development  
Sandia Laboratories  
P. O. Box 5800  
Albuquerque, NM 87185

	<u>BNL Distribution</u>
DNE Chairman	(1)
DNE Deputy Chairman	(1)
RSP Associate Chairmen	(3)
Safety Evaluation Group	(14)
Nuclear Safety Library	(2)